PREDICTING NON-LINEAR BENDING BEHAVIOUR OF ULTRA-THIN WOVEN FIBRE COMPOSITES

Hasitha Sithadara Wijesuriya

188035A

Degree of Master of Science

Department of Civil Engineering

University of Moratuwa
Sri Lanka

September 2019

PREDICTING NON-LINEAR BENDING BEHAVIOUR OF ULTRA-THIN WOVEN FIBRE COMPOSITES

Hasitha Sithadara Wijesuriya

188035A

Thesis submitted in partial fulfilment of the requirements for the degree of Master of Science in Civil Engineering

Department of Civil Engineering

University of Moratuwa
Sri Lanka

September 2019

Declaration

I declare that this is my own work and this thesis does not incorporate without acknowledgement any material previously submitted for a Degree or Diploma in any other University or institute of higher learning and to the best of my knowledge and belief it does not contain any material previously published or written by another person except where the acknowledgement is made in the text.

Also, I hereby grant to University of Moratuwa the non-exclusive right to reproduce and distribute my thesis, in whole or in part in print, electronic or other medium. I retain the right to use this content in whole or part in future works (such as articles or books).

..... Date :

H.S.Wijesuriya

The above candidate has carried out research for the Masters thesis under my supervision.

..... Date :

Dr. H.M.Y.C. Mallikarachchi

Abstract

Ultra thin woven composites are extensively used in deployable space structures, particularly on deployable booms which are responsible to deploy and hold key components in space missions. Due to high weight sensitivity of these applications, it is essential to achieve the maximum structural efficiency to reduce the payload. However the flexural behaviour of these thin textile composites is still troublesome under high curvatures. Hence it limits the optimization of deployable structures to highest degree possible.

Numerical modelling of these structures is considered as a promising tool in designing, considering the time consuming and costly nature of physical testing. Yet, most of the numerical models aimed at the macroscopic behaviour, suffer from lack of accurate behavioural characteristic of non-linear geometric regime.

This study is an attempt made to address the above problem by building virtual simulation techniques through micromechanical modelling. For this work a homogenized Kirchhoff Love plate model was developed with the identified unit cell of two-ply plain weave composite. The geometry was imported from TexGen textile modelling package and FEA simulation was done by ABAQUS commercial finite element package.

A new logical framework was proposed to describe the behavioural characteristics of the tows at the interlacing points by means of cohesive behaviour. Material definition for cohesive interaction was included through traction separation law maximum principal stress criterion for damage initiation. Required traction coefficients were extracted by a discrete FEA simulation due to unavailability of experimental data.

The developed model was executed in the linear regime and then extended to non-linear geometric regime to predict the flexural behaviour under high curvatures and it shows bending stiffness reduction as expected. Thus the proposed simulation technique can be utilized in designing process of deployable booms made of thin woven composites through the multiscale modelling approach after verifying the accuracy with experiments.

Keywords : *ultra-thin fibre composites, woven composites, non-linear bending behaviour, representative unit cell, ABD matrix, cohesive behaviour, traction separation, damage criterion*

Dedication

To my parents and brother, without whom none of this would be possible.

Acknowledgement

First and foremost, I would like to express my sincere gratitude to my supervisor Dr. Chinthaka Mallikarachchi, for his technical guidance and valuable insights throughout the past year. Without his support, this would have not been possible. I would also like to express my gratitude for the valuable comments and advice given by professor Priyan Dias and professor Rangika Halwatura during progress reviews.

Next, my gratitude goes to the academic staff members of Department of Civil Engineering of University of Moratuwa. My sincere appreciation to Isuru Nanayakkara, Milinda Yapa, Mierunalan Seyon, Varakini Sanmugadas, Chamith Deemantha, Vishnu Punithavel, Sahangi Dassanayake, Sujeeka Nadarajah and Hasini Weerasinghe for being great research colleagues and for their support and helpful conversations throughout my research work. I am grateful to everyone who helped in any way possible to make this a success.

Finally, I would like to thank Ceylon Steel Corporation (Pvt.) Ltd., National Research Council, Sri Lanka and Senate Research Committee of University of Moratuwa for the financial assistance provided.

Contents

List of Figures

List of Tables

Nomenclature

List of Abbreviations

C3D6 3D continuum six-node wedge elements

C3D8 3D continuum eight node brick elements

DLR German Aerospace Center (Deutsches Zentrum fr Luft- und Raumfahrt e.V.)

DSL Deployable Structures Laboratory

ESA European Space Agency

LEFM Linear Elastic Fracture Mechanics

MARSIS Mars Advanced Radar for Subsurface and Ionospheric Sounding

NASA National Aeronautics and Space Administration

PBC Periodic Boundary Conditions

RUC Representative Unit Cell

XFEM Extended Finite Element Modelling

List of Symbols - Roman

1K Thousand filament tow

A Cross sectional area of tow

a Tow thickness

E_1 Longitudinal stiffness

E_2 Transverse stiffness

E_m Stiffness of matrix

G_{12} Shear stiffness

G_{23} In-plane shear stiffness

K_{nn} Traction stiffness in normal direction

K_{ns} Coupling of traction stiffness in normal and shearing direction

K_{nt} Coupling of traction stiffness in normal and tearing direction

K_{ss} Traction stiffness in shearing direction

K_{st} Coupling of traction stiffness in shearing and tearing direction

K_{tt} Traction stiffness in tearing direction

M Out-of-plane moment resultant

N In-plane force resultants

P Force just before the failure in platen folding test

$S22$ Normal stress of 2 plane in 2 direction

t_n Traction stress in normal direction

t_s Traction stress in shearing direction

t_t Traction stress in tearing direction

u Displacement in X direction

v Displacement in Y direction

V_f Fibre volume fraction

W Aerial weight of fabric/film

w Displacement in Z direction

w_s Width of the specimen

List of Symbols - Greek

α_0 Stiffness reduction factor

δ_n Separation in normal direction

δ_s Separation in shearing direction

δ_t	Separation in tearing direction
Δl	Weave length of RUC
δ	Distance between two plates - platen folding test
γ	Shear stress
κ_x	Curvature around X axis
κ_y	Curvature around Y axis
κ_{xy}	Twisting curvature
κ	Out-of-plane curvature
ρ	Density
υ_{12}	Poisson's ratio
υ_m	Poisson's ratio of matrix
ε_x	Strain in X direction
ε_y	Strain in Y direction
ε_{xy}	In-plane shear strain
ε	In-plane strain

Chapter 1

Introduction

1.1 History and Development of Composites

Composite materials were used by earliest stages of civilizations, even though their rapid development only took place in the mid 20^{th} century. Use of straw to strengthen mud bricks by ancient middle eastern civilizations and use of rearranged wood panels by ancient Egyptians, are only a few earliest attempts to achieve superior strengths and resistance to expansion and swelling of structures through the combination of materials. This suffices the knowledge they had on the manipulation of materials in order to cater their needs. From those prehistoric times, composite materials have evolved dramatically over the past century.

With the discovery of high-quality synthetic adhesive materials in early 20^{th} century, composite materials took a new turn by entering to the aerospace industry. Figure 1.1 shows the British twin-engine de Havilland DH.98 Mosquito aircraft constructed in 1940 mostly with laminated plywood, representing the extreme point of engineering with composite materials[1].

Figure 1.1: de Havilland DH.98 Mosquito aircraft
(courtesy: Canadian Forces)

Accidental discovery of a mass production method for fibreglass in 1950′s paved the way for current state of fibre composite materials, even though it was only used for thermal insulation applications at the time. With the development of kevlar and carbon fibre production methods fibrous composites now dominate every engineering application ranging from aerospace to automotive engineering domain, Figure 1.2. Main reasons for this popularity is the higher strength and stiffness to weight ratios, better thermal and acoustic insulation and high resistance to fatigue.

Figure 1.2: McLaren F1 - first production car with CFRP monocoque chassis (courtesy: McLaren Automotive)

1.2 Woven Fibre Reinforced Composites

As the name implies woven fibre composites consist of two basic constituents; fibre and matrix material which holds together individual fibres in tows and laminae. Tow is a bundle of filaments made out of fibres, i.e. carbon, glass or aramid, which acts as the main component of load transferring mechanism. These tows are weaved in order to make a fabric so that it resides higher intra lamina strength over the uni-directional lamina. There are different kinds of weave patterns ranging from plain weave to 3D woven to match specific requirements. Figure 1.3 illustrates a schematic of the components of plain-weave fabric.

Due to tailorable material properties and high strength and stiffness to weight ratios of fibre composites, they have gained a huge popularity as a structural material specially for weight sensitive applications as stated in Section 1.1. Since woven fabrics possesses better inter lamina strength and

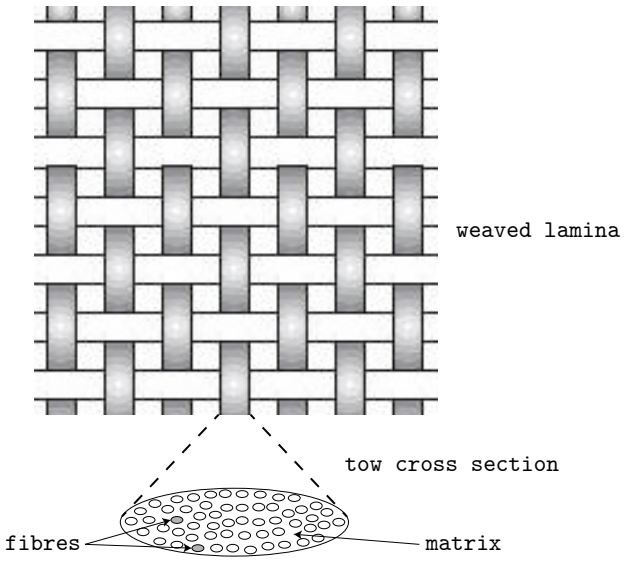

Figure 1.3: Schematic of a plain-weave woven fabric

higher damage tolerance properties over composites made of uni-directional lamina, it has been used extensively for space applications over the past few decades.

With the emerging new concepts like use of solar radiation to propel spacecrafts, need of larger diameter mirrors and lengthier antennas to observe deep space required to have large space structures. Yet the limit imposed by the launch vehicle both, of size and weight was a critical constraint in development of those missions. Figure 1.4 gives a clear idea on the space limit imposed by the transportation medium. Then the concept of deployable structures emerged which allows to pack a large structure into a compact configuration for stowage and then expand back to the required configuration once in space. Some of these deployable mechanisms include mechanical actuators, inflatables and deployable booms.

Deployable booms made of ultra-thin composites can be folded elastically and are able to propel back to original state using the stored strain energy during folding. Due to the superior damage tolerance and de-lamination properties, of woven fibre composites as well the ability to function in harsh environments, makes woven composites an ideal candidate for ultra thin deployable booms. As shown in Figure 1.4(a) the spring reflector is thin enough, even one can see through the structure itself. Figure 1.5 illustrates the fully

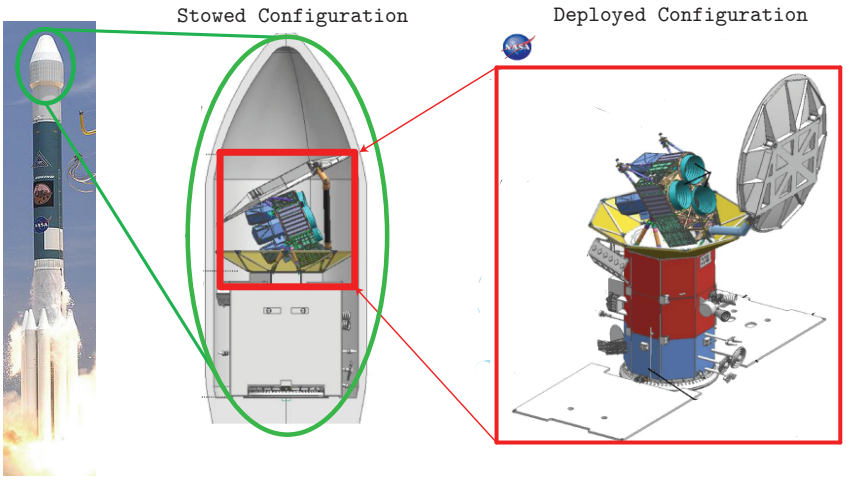

Figure 1.4: Stowage configuration of a satellite (courtesy: NASA)

deployed state to folded state of a tape spring made with woven composite.

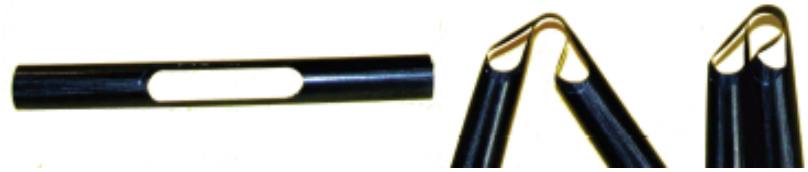

Figure 1.5: States of tape spring in self-deployment

These deployable structures has been used in some space missions successfully and it is being proposed to use the same approach in future space missions too. Antenna used for sounding radar of MARSIS is first of its kind which was used to identify the different layers of material in Mars's subsurface[2]. In order to emit sound waves with high wavelength it has to have antennas of 40 m. This high length antenna requirement was only be possible by packaging it into a stowed configuration as shown in Figure 1.5. This was achieved by introducing slots in certain interval and folding the antennas.

1.3 Challenges

As discussed in Section 1.2 those deployable booms are going through high deformation in both folding and deployment process. It is clearly shown by Figure 1.4 and Figure 1.5, that those structures undergoing into geometrically non-linear regime in order to achieve these high curvatures. Due to this geometric non-linearity and dynamic behaviour of booms, it is a tedious task to

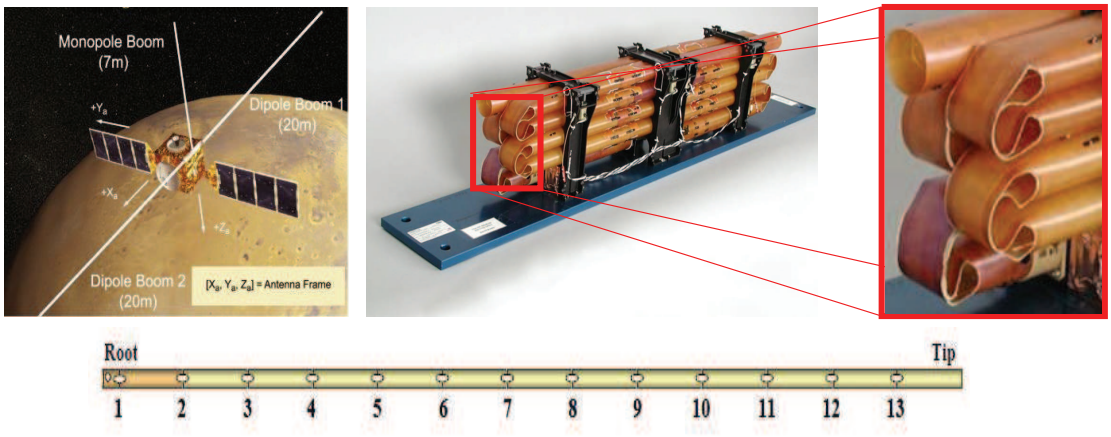

Figure 1.6: MARSIS boom
(courtesy: ESA)

capture the exact behaviour of booms through physical experiments.

1.3.1 Testing in virtual environment

Since these structures are crucial components for the success of a space mission generally costing in millions of US Dollars, it is essential to identify and understand the mechanical behaviour of them beforehand. Gravity and air-drag during the experiments, which are unavoidable in laevorotatory conditions affects the results of these experiments involving stored energy deployable booms. Also time consuming, costly and repeated nature of physical experiments leads to an alternate that can be utilized in design optimization that may require several design cycles.

In virtual testing methods, the first approach is employing numerical models to capture the behaviour of these thin-walled structures. Since available commercial finite element software packages are able to handle more complex contact and discontinuities involved, it has been widely used in simulating these kind of structures[3, 4]. Soykasap [3] and Mallikarachchi et al.[4] show that these thin walled structures are undergoing significant bending moment reduction when it folds to high curvatures. However this behaviour is yet to be captured via simulations.

1.3.2 Lack of an analytical method

Classical Lamination Theory (CLT) has been used for decades to analyse and design laminated composite structures. It was proven to be working perfectly in the analysis of uni-directional laminae. But it cannot be directly used in the case of woven fibre composites due to the assumptions in the theory itself. CLT assumes the mid plane as the reference plane i.e fibres are distributed evenly across the thickness of lamina and a constant thickness throughout the lamina. Further its homogenized properties are calculated by integrating across the thickness[5]. Clearly, none of the above assumptions can be directly imposed to woven fabrics due to there woven nature.

Le Page et al.[6] and Naik[7] have used analytical method based on CLT and it captures the in-plane properties quite well, but fails to capture the flexural properties, particularly for ultra thin woven fibre composites. Karkainen and Sankar[8], and Soykasap[3] noticed that the direct use of CLT causes an over prediction of bending stiffness by 300% to 400%.

1.4 Scope and Aim

The broad aim of this research is to develop a micro-mechanical model for ultra thin woven fibre composite unit cell which can capture the flexural behaviour in non linear geometric regime. Thus the developed model can be utilized to designing and simulating ultra thin deployable booms made of woven fibre laminae through multi-scale modelling.

This work is based on a two-ply plain weave fibre composites made of 1000 filament carbon fibre tows embodied in an epoxy matrix. From section 1.3 it is evident that it is essential to look at micro-mechanical behaviour to predict the macroscopic behaviour of these structures. Due to lack of proper understanding of the woven composites, current designs of textile structures are not fully optimized for maximum damage resistance and light-weight.

First a suitable repeating unit cell was identified to build a micromechanical model of two-ply plain weave laminate. Then geometric features of the unit cell was measured through available micro-graphs[9]. Idealization of geometry is a crucial part since many have tried different idealization techniques and yet

failed to capture the exact behaviour[8, 10, 11]. This study has followed a different approach by using a textile modelling software named TexGen, to generate the geometry of the unit cell. A more realistic elliptical cross section was chosen to represent the exact geometry of the tow cross section. Subsequently, a Representative Unit Cell (RUC) was built in ABAQUS commercial finite element package with the imported geometry from TexGen.

As illustrated in Figure 1.3 plain weave fabric has two sets of tows interlacing at 90° acting as the reinforcement of the material. These crossover points were modelled using cohesive interaction property and damage parameters was adopted to simulate the behaviour caused by going into non-linear geometric regime under high curvatures. The cohesive interaction between interlacing tows was modelled using the extracted traction coefficient values through a distinct fracture simulation of epoxy matrix.

The developed RUC model was first analysed in the linear regime using ABAQUS/Implicit solver to check the validity of the results. Upon validation of the extracted stiffness values in linear regime it was further implemented in the non-linear regime.

1.5 Chapter Organisation

This thesis consists of 6 chapters. After the current introductory chapter, Chapter 2 gives an overview of literature on micro-mechanical modelling and past studies on characterising their flexural behaviour numerically. First it describes the theory behind the constitutive of ultra-thin plates and then it gives a detailed description on available studies carried out so far. Finally it gives a brief review on the multi-scale modelling and its applicability on this study.

Chapter 3 is based on the steps taken in building the geometry of the RUC. First it gives methodology on obtaining the isotropic material properties of the tow which is a combination of fibres and epoxy. Secondly it presents the steps followed on obtaining the geometric parameters of the weave and tow cross section followed by the idealization of the geometry in TexGen textile modelling software.

Chapter 4 describes the behavioural identification at the cross over points of the weave. It identifies the possible characteristics at those points when the boom is undergoing an extreme curvature and build the hypothesis of cohesive behaviour based on that. Then it presents a new modelling technique to capture the relative slip of the tows with the use of cohesive interaction modelling and damage initiation criterion.

Chapter 5 presents how the RUC was built in the ABAQUS incorporating Periodic Boundary Conditions (PBC) and using the exported geometry from TexGen which was described in Chapter 3 and the cohesive material properties extracted in Chapter 4. Then it shows the obtained results of a linear analysis and verifies the results with experimental data. Finally it presents the results in non linear analysis and compares with the experimental data presented in Chapter 2.

Chapter 6 concludes the thesis with suggestions for future research directions.

Chapter 2

Literature Review

This chapter presents an overview of literature on ultra-thin deployable booms. The chapter begins with a brief overview on the deployable booms. Then a review on analytical methods adopted in analysing thin woven composites is presented. Next part is utilized to present a review on recent developments of micro-mechanical simulation techniques. Finally it gives an overview on the multi-scale modelling and its applicability on this study. Though there are many self deployable systems available, this chapter is mainly focusing on the thin-walled tubular booms.

2.1 Stored-Energy Deployable Space Structures

Deployable booms have gained their popularity as a deployable mechanism for space missions mainly due to two reasons, first one is the low weight compared to its counterparts and higher reliability of the components being the second fact. since their functionality do not depend on external sources. Unlike mechanical motors and actuators, their functionality totally depends on the stored strain energy in the folding process. This self-deployable nature without permanent deformations is what makes them an ideal candidate for high precision large space systems.

2.1.1 Deployable booms

Most space systems are equipped with deployable booms to deploy and support peripheral structures like large antenna reflectors, solar sails for propelling and solar arrays to generate power. These booms can be categorized by its purpose and physical parameters. Deployable booms can be categorized into thin-walled tubular booms, telescopic masts, coilable masts and articulated trusses [12]. The methodology used by each category depends on the application. Figure 2.1

illustrates a step wise demonstration on deployment of an articulated truss.

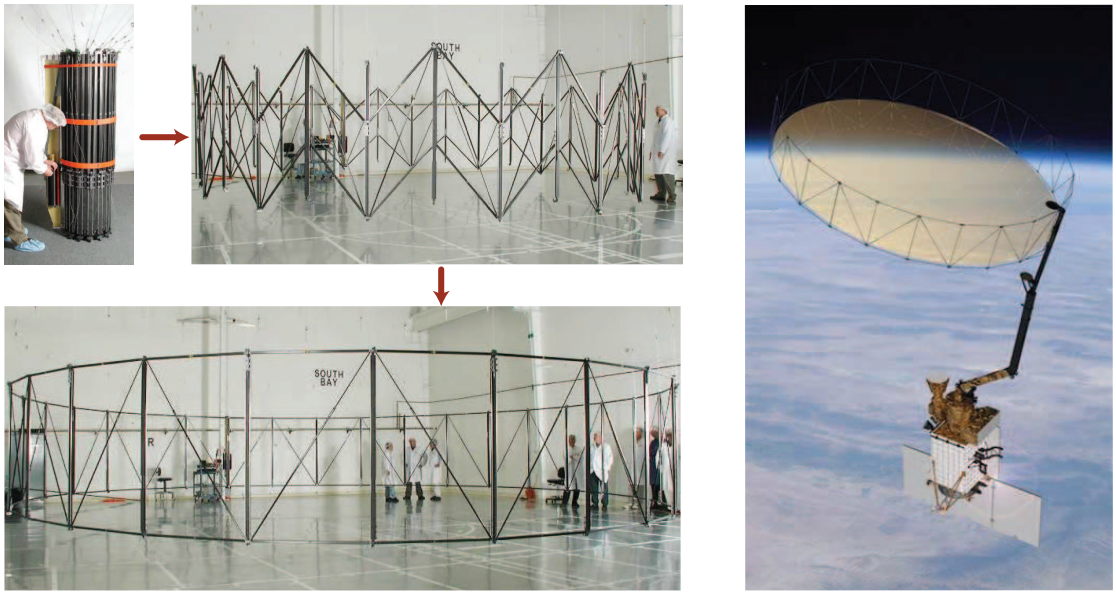

(a) (b)

Figure 2.1: Astro Mesh 2 (courtesy: Astro Aerospace)
(a) Stages from folded to deployed configuration (b) Final step with reflector attached

Tape springs

Tape springs are the simplest form of stored energy deployable structure which was developed upon the same concept as in carpenter steel measure tapes. Its simplicity is one of the main advantages over mechanical hinges with moving parts which can be jammed during the operation. As well tape springs possesses a higher stiffness in deployed state due to its inherent curvature, making it a robust deployable mechanism for space missions.

Their behaviour can be characterised by observing moment-rotation curve. This behaviour is linear in small rotations and does have a constant moment when a large rotation occurs. Tape springs can be flipped either in equal sense or opposite sense to the transverse curvature, Figures 2.2(a) and 2.2(b). Hence the behaviour depends on the direction of applied moment [13]. In general notations, moment is considered positive in opposite sense bending and vice versa. As shown in Figure 2.2(c) maximum moment in opposite sense is much larger than that of equal sense. When positive moment is applied, after the linear regime of OA the tape suddenly snaps and forms a smooth localized curved portion at the middle followed by constant moment with the increasing arc length at the middle. In

the unfolding sequence it follows same path from CB extending that till D and suddenly snaps to E. When a negative moment is applied tape undergoes the similar path but with a lesser peak moment and it follows the same path as folding in the unfolding process too.

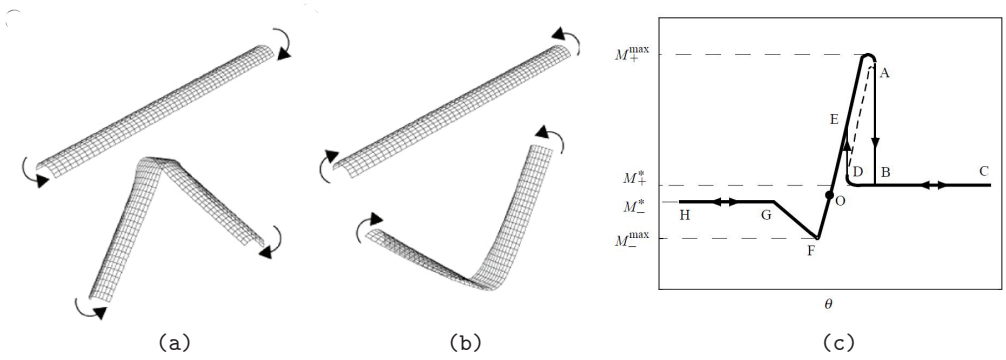

Figure 2.2: Bending of tape spring [14, 15]
(a) Equal sense (b) Opposite sense (c) Typical moment rotation curve

It is evident that maximum moment in opposite sense bending is higher than that of equal sense bending. Therefore two or more spring tapes are combined in opposite orientation as a countermeasure for post-latching dynamic behaviour; folding in the opposite sense that was originally bend in the equal sense due to high kinetic energy in deploying. Figure 2.3 shows an instance where the tape springs are used as the deploying mechanism. The arrangement gives a great torsional resistance due to the offset springs too.

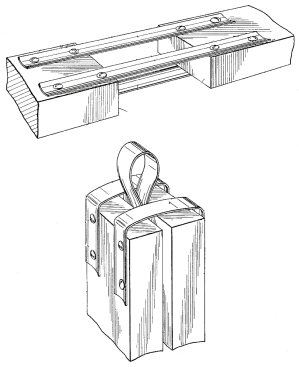

Figure 2.3: Bending of tape spring [16]

Though the earlier tape springs are made out of metal alloys, now there is a trend to use fibre reinforced composites due to its higher strength, stiffness and tailorable properties.

Tape spring hinges

With the demanding requirements from space missions, there is a tendency of making monolithic structures, i.e. entire component embedded in the deploying mechanism. Figure 2.4 shows two examples for on that.

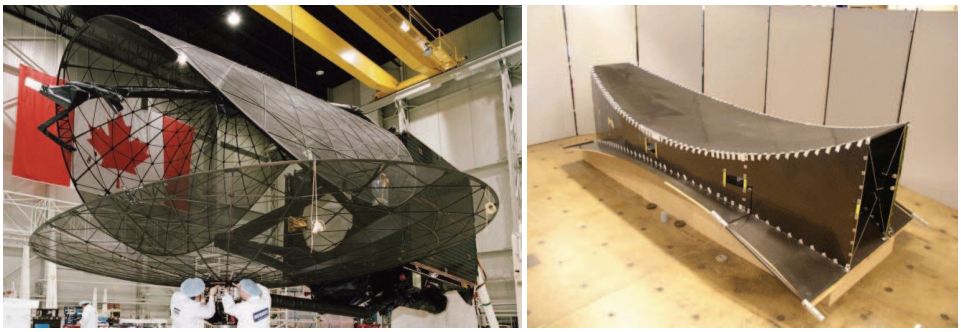

(a) (b)

Figure 2.4: Foldable reflector antennas
(a) Spring back reflector (b) Deployable reflector (courtesy: (a) Boeing (b) DSL)

As presented in Figure 1.3 all three antennas of MARSIS are manufactured with one single piece of composite tube. These tubes are slotted in certain intervals as shown in Figure 2.5.

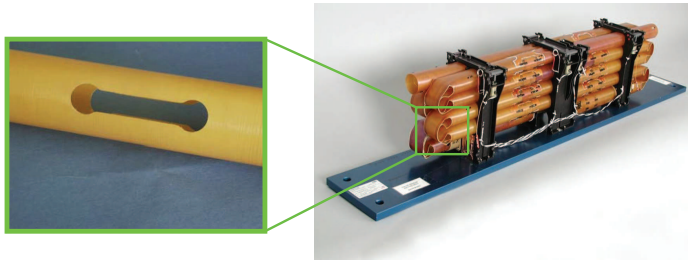

(a) (b)

Figure 2.5: Configuration of a MARSIS antenna (courtesy: Astro Aerospace)
(a) Hinge (b) Antenna in stowed configuration

In 2011, Mallikarachchi [9] simulated the quasi-static deployment behaviour for the tape spring hinge made out of two ply plain weave fibre composite (like the one shown in Figure 2.5 (a)). Physical behaviour of the boom have successfully captured with the developed simulation. However moment rotation relationship was not captured well in the deployment angle of 20° to 0° even though a modified bending stiffness parameter was used in the analysis, Figure 2.6. Ubamanyu [17] simulated the quasi-static behaviour of a dual-matrix composites boom, i.e. boom made out of softer matrix at the hinge regime and traditional epoxy matrix elsewhere, by reducing the bending

stiffness to 10%, 50%, 100%. It was revealed that the bending moment is changing with the curvature once the modified simulation were compared with the results of the experiment carried out by Sakovsky [18].

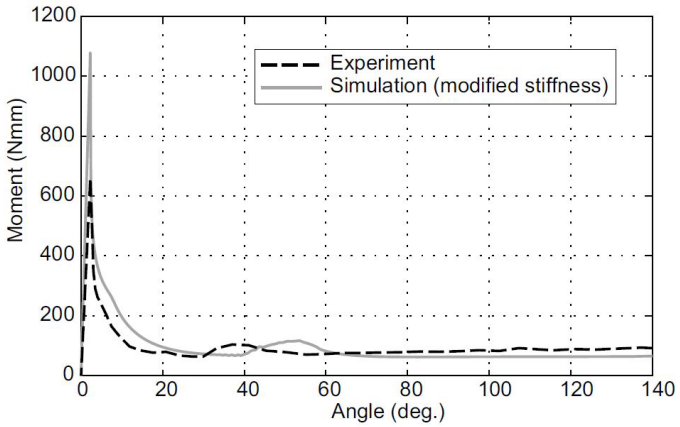

Figure 2.6: Comparison of moment rotation during deployment of tape spring hinge [9]

2.1.2 Non-linear experimental data

Mallikarachchi [19] introduced a new failure criterion in terms of force and moment resultants and the failure coefficients were obtained with physical testing in order to validate the failure locus. Four point bending test was conducted to obtain the initial bending stiffness of composite till 0.01 mm^{-1} of curvature. Since the elastic deformation for thin laminates are too large a platen folding test was performed until the failure, in order to obtain the smallest radius and the corresponding load that a laminate can be folded before failure, Figure 2.7.

Initial bending stiffness predicted from the four point bending test is 37.55 Nmm with a standard deviation of 5.54 Nmm [9]. At failure, bending moment (M_x) and the corresponding curvature (κ_x) was calculated from the method proposed by Sanford and Biskner [20] based on Euler's Elastica, Equation 2.1 and 2.2.

$$\kappa_x = \frac{2.3963}{\delta} \tag{2.1}$$

$$M_x = \frac{0.8346\ P\delta}{w_s} \tag{2.2}$$

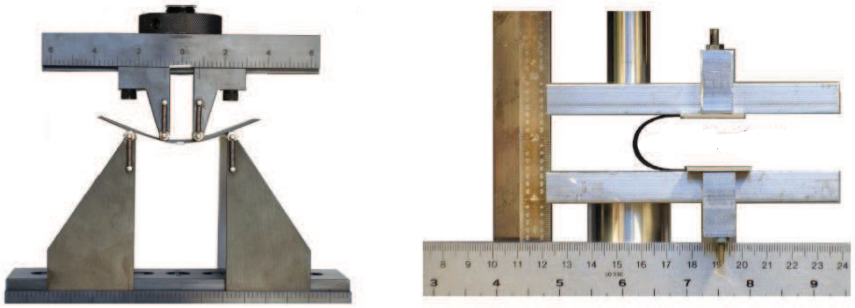

(a) (b)

Figure 2.7: Bending experiment setups [19]
(a) Four point bending test (b) platen folding test

From a series of tests, extracted κ_x and M_x just before the failure was 0.203 mm^{-1} and 5.068 Nmm/mm with a standard deviation of 0.01 mm^{-1} and 0.293 Nmm/mm respectively. Figure 2.8 illustrates the positioning of initial bending behaviour curve and failure moment on the same graph.

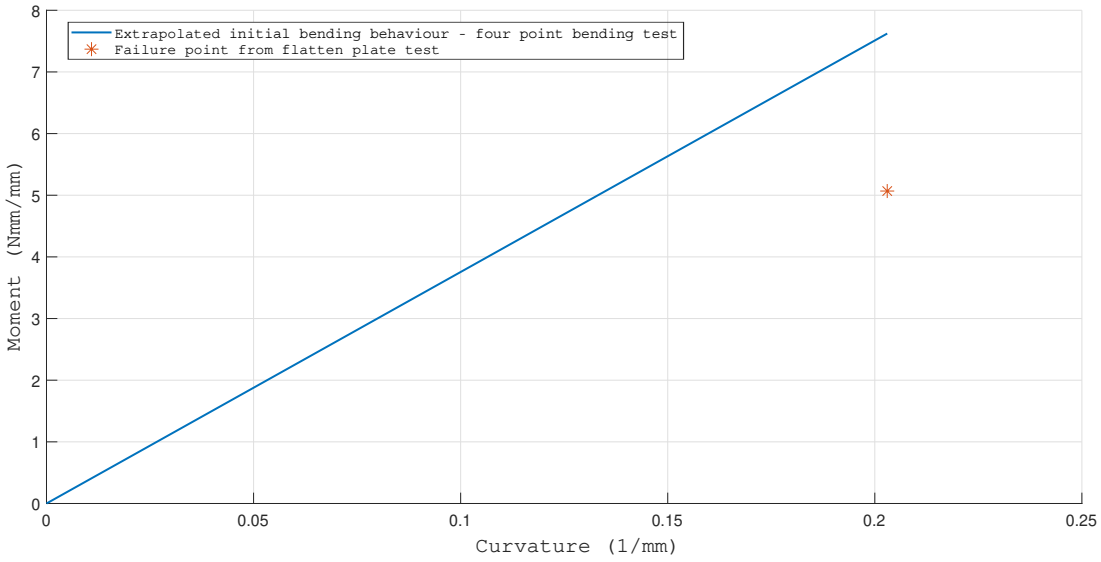

Figure 2.8: Bending stiffness - experimental results [9]

From the initial bending stiffness value extracted from four point bending test, moment at failure should be 7.622 Nmm/mm whereas from the experimental data it is only 5.068 Nmm/mm. Hence the bending moment is reduced by more than one third according to the results. Average stiffness reduction factor (α_0) for the samples is 0.6.

2.2 Analytical Approach

Behaviour of laminates can be predicted analytically by analysing the lamina, to get the end result as a constituent law. This theory is called Classical Lamination Theory often abbreviated as CLT. CLT is developed upon a collection of hypothesis and validity of those hypothesis to woven composites are discussed in detail.

2.2.1 Classical Lamination Theory

The theory is based on the Kirchhoff-Love hypothesis for shells. The steps for analysing a particular laminate is as follows. First, individual lamina is analysed and expressed the constituent by relating in plane stresses to in plane strains and out of plane curvature. Then the resultant force on laminate is obtained by integrating the corresponding force and moment through the thickness of all the laminae resulting the formation of ABD matrix [21]. ABD matrix is the standard 6×6 constituent matrix for describing the behaviour of any laminate material. ABD matrix is presented in Equation 2.3 in a compact form.

$$\begin{Bmatrix} N \\ \cdots \\ M \end{Bmatrix} = \begin{pmatrix} A & | & B \\ \cdots & \cdots & \cdots \\ B & | & D \end{pmatrix} \begin{Bmatrix} \varepsilon \\ \cdots \\ \kappa \end{Bmatrix} \tag{2.3}$$

where, N denotes in plane force resultants, M denotes out of plane moment resultants and ε and κ denotes in plane strains and out of plane curvatures respectively. ABD matrix is consists with 3 sub matrices of A, B and D, each consisting with 9 elements. A matrix denotes the relationship of extensional parameters (in plane force resultants and strains). D matrix denotes the relation of bending parameters (out-of-plane moment resultants and curvatures) where B sub matrix denotes the coupling between bending and extension parameters. Expanded ABD matrix denoting the relationship of all the in plane forces, out of plane moments and in plane strains, out of plane curvatures are presented in Equation 2.4. x and y denote the two principal directions of the laminate.

$$\begin{Bmatrix} N_x \\ N_y \\ N_{xy} \\ \cdots \\ M_x \\ M_y \\ M_{xy} \end{Bmatrix} = \begin{pmatrix} A_{11} & A_{12} & A_{16} & | & B_{11} & B_{12} & B_{16} \\ A_{21} & A_{22} & A_{26} & | & B_{21} & B_{22} & B_{26} \\ A_{61} & A_{62} & A_{66} & | & B_{61} & B_{62} & B_{66} \\ \cdots & \cdots & \cdots & \cdots & \cdots & \cdots & \cdots \\ B_{11} & B_{12} & B_{16} & | & D_{11} & D_{12} & D_{16} \\ B_{21} & B_{22} & B_{26} & | & D_{21} & D_{22} & D_{26} \\ B_{61} & B_{62} & B_{66} & | & D_{61} & D_{62} & D_{66} \end{pmatrix} \begin{Bmatrix} \varepsilon_x \\ \varepsilon_y \\ \gamma_{xy} \\ \cdots \\ \kappa_x \\ \kappa_y \\ \kappa_{xy} \end{Bmatrix} \tag{2.4}$$

Assumptions in CLT

Assumption made in deriving CLT are derived from Kirchhoff-Love hypothesis for shells. Main assumptions is, the middle sections of the laminate are presumed to remain straight and perpendicular to middle surface when the laminate is extended or bend. As a consequence shear stresses perpendicular to the middle surface should be zero, i.e. $\gamma_{xz} = \gamma_{yz} = 0$. With that, it is assumed that the bonds are infinitesimally thin and non-shear deformable; laminae cannot slip relatively each other. As well thickness of individual lamina is presumed to be constant in the calculation of ABD matrix by integrating the forces and moments through the thickness.

CLT with woven textiles

Due to the inherent patterns of weave, most of the above stated assumptions are not valid to woven textiles. Due to the geometry and the interlacing of tows, a lamina made of woven fibre is not constant in thickness. As stated in Section 2.2.1, resultant forces and moments are taken performing an integration through the thickness. Hence the D matrix is highly dependent on the thickness of the laminae. Karkkainen and Sankar [8] performed an analysis of two-ply plain weave composites with CLT and found that the bending stiffness is over predicting by about 300%. And study done by Soykasap [10] revealed that the prediction of maximum bending stiffness by CLT gives an error upto 400%. Thus based on these studies and the concepts of micro-mechanics, it is clear that the CLT is not suitable on predicting the flexural behaviour of the composites.

It is clear that the behaviour of woven fibre composites can not be

characterized in the macro length scale due to its complex architecture. Therefore it is required to go into a smaller length scale in order to capture the exact behaviour.

2.3 Multiscale Modelling

Multiscale modelling is a branch which is considering important features of multiple scales in time and space in order to solve a problem. This is widely used in solid mechanics, chemistry and biology. This concept was first developed in 1990′s to simulate the performance of nuclear weapons with the rising concerns on performing physical nuclear tests. From that era onwards, multiscale modelling was developed in a fast phase and proved its usefulness in many areas involving complex iterative simulations which were limited to theories earlier [22]. With the advancement of the field, engineering design has achieved most out of it through the High Performance Computing (HPC) [23]. Now it is possible to simulate large structures, components like of an aircraft, accurately and efficiently through the use of multiscale simulation. Figure 2.9 illustrates the advancement of engineering design through an example.

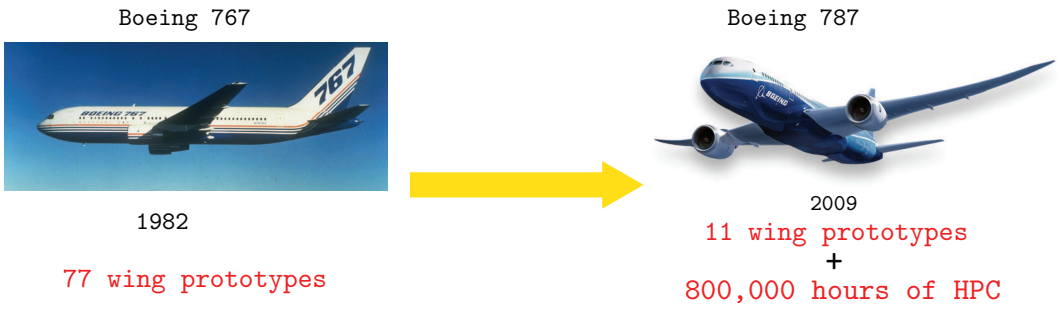

Figure 2.9: Reduction of aircraft wing prototype testing in the design process

This concept can be adopted to the simulation of booms made out of ultra-thin woven fibre composites. Schematic in Figure 2.10 shows the methodology that can be adopted in order to characterize the behaviour of the boom through the use of RUC of the textile composite. This process is iterative where the constituent of the boom is constantly updating with the analysis results from the boom with respective to the displacement and rotation parameters of the deformed shape of the boom [24].

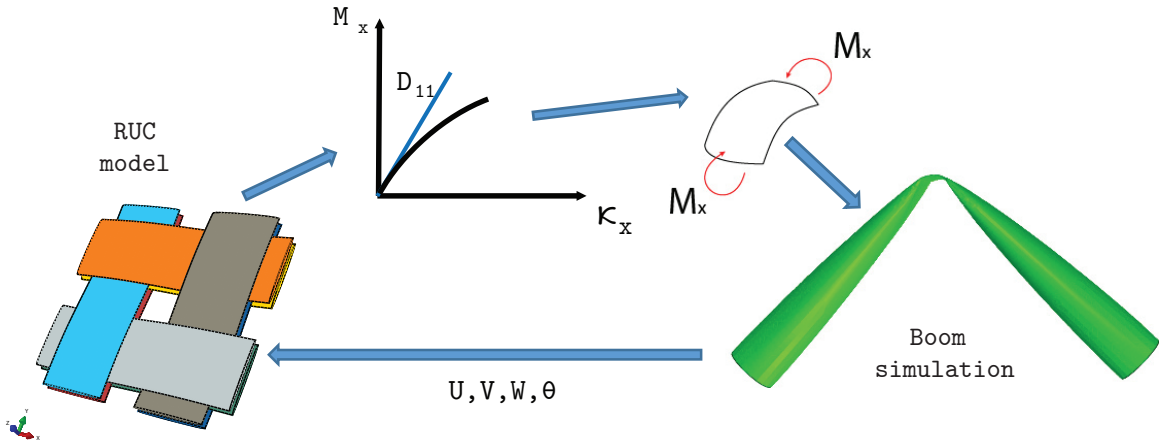

Figure 2.10: Multiscale simulation technique

2.4 Micromechanicanical Modelling of Woven Textiles

It is essential to identify the micro mechanical behaviour of woven fibre composites to utilise multiscale modelling technique for the accurate prediction of macroscopic behaviour. Numerous studies have been conducted so far to capture the accurate mechanical behaviour of those composites in micro state. On those studies various attempts were made to idealize the RUC to replicate the physical behaviour accurately.

RUC can be described as a repeating pattern of the weave geometry when it comes to mesoscale of textiles. It depends on the tow arrangement and ply arrangement. Figure 2.11 shows RUC of plain weave and triaxial weave geometry.

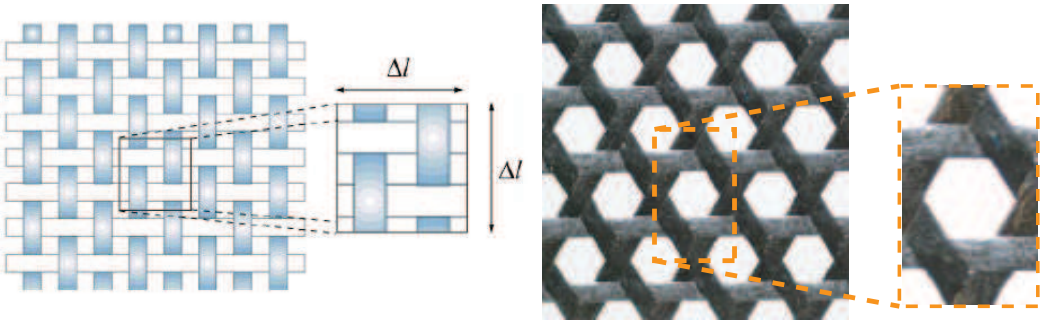

(a) Plain weave (b) Triaxial weave

Figure 2.11: Identification of RUC in woven textiles

Studies based on the RUC model dates back to 1980′s. Ishikawa and Chou [25] idealised the textile laminate with series of plates which represent the cross-ply laminates. This model is lacking the representation of interlacing

points. This work was further extended by introducing the fibre undulation, so that it represents the continuity of the fibres [26].

Cox et al. [27] developed a new model by integrating 1D line elements to represent the individual fibres in a tow. McGlockton [28] extended this work further and predicted the stiffness properties accurately.

In 2006, Karkkainen and Sanker [8] developed a direct micro-mechanical based FEM model for a plain weave lamina. This model considers the bending effects for the first time and it uses Kirchhoff-Love theory for shells for homogenization. As well it adopted PBC to represent the repeating nature of RUC. Therefore the constitution relationship was obtained as the ABD matrix which is the universally adopted to represent laminates. Figure 2.12 represents their RUC.

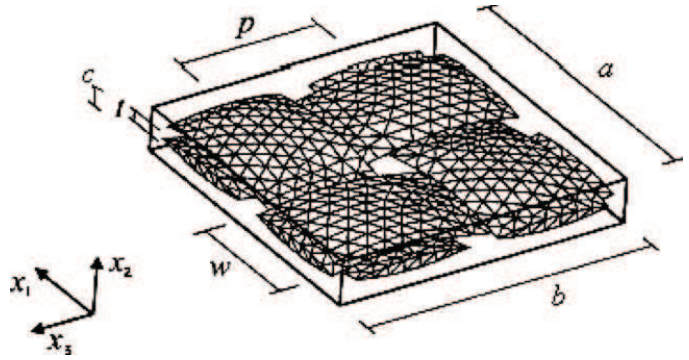

Figure 2.12: RUC of plain weave laminae made with solid elements [8]

Kueh and Pellegrino [29] adopted the same method and modelled triaxial weave fabric with 1D beam elements, Figure 2.13. Crossover points were connected through multipoint constraint to make sure there is no relative movement in tows at interlacing points. With experimental data for the same material, the obtained mechanical properties of the simulation was validated. Tensile, Compressive, shear and bending stiffness in the linear geometric regime were captured accurately through the developed simulation.

In 2011, Mallikarachchi [9] applied the above method to two-ply plain weave composite laminate. The tow weave geometry was assumed as fourth root of sine curve. This model was built with the adhesive material in-between the tows to idealize the exact behaviour of the composite. As well a series of reference

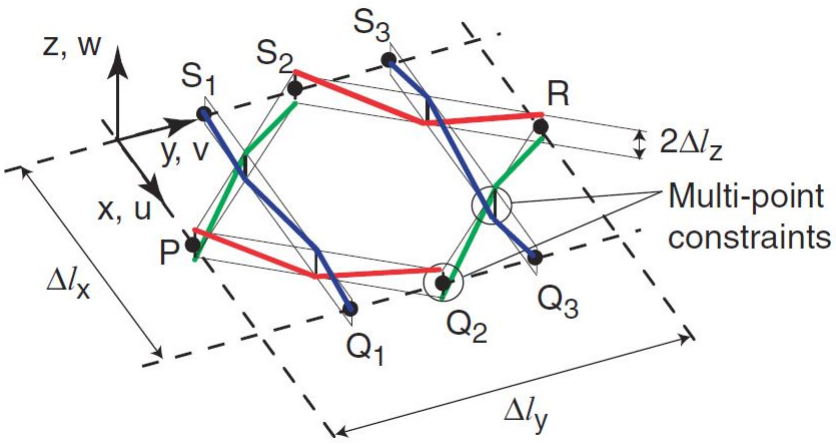

Figure 2.13: RUC of triaxial weave fabric with beam elements [29]

points were used instead of one to connect the tow boundary to the respective dummy nodes, Figure 2.14. This eliminates the formation of rigid plate at the boundary face when there is only one reference point connecting the whole face. Obtained stiffness values from the developed model matches the results obtained from a series of experiments proving the validity of the model in linear regime.

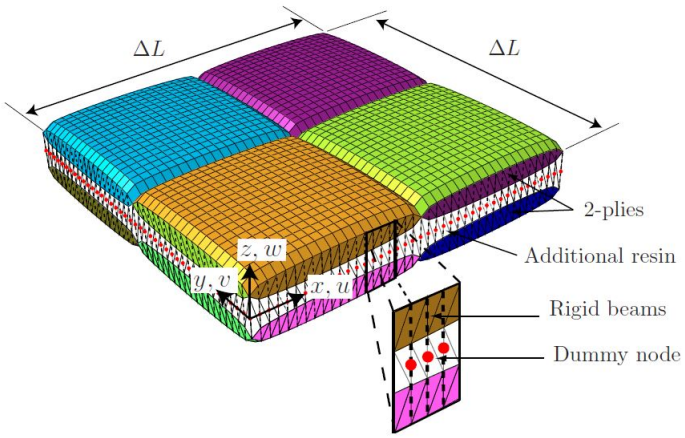

Figure 2.14: RUC of two-ply plain weave composite made with solid elements [9]

As presented by Section 2.1.2 in two-ply plain weave composites, a reduction of bending stiffness was observed with the curvature. Yapa and Mallikarachchi [11] attempted to capture the bending behaviour with 1D beam element model. The interlacing points were modelled with deformable beam elements. Results from their simulation and experiment conducted by Mallikarachchi [9] are plotted in the same graph, Figure 2.15.

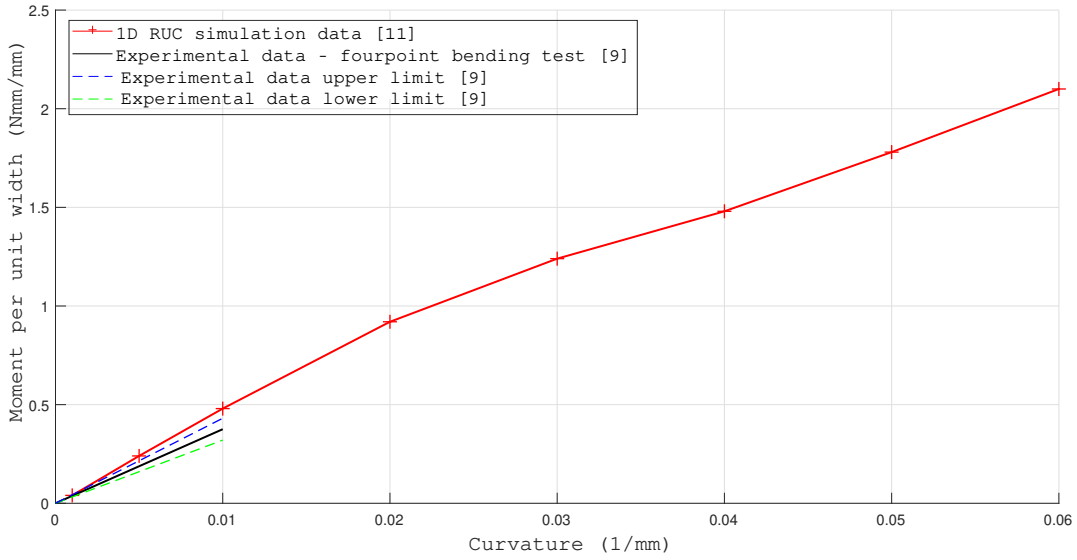

Figure 2.15: Moment vs. curvature graph [11, 9]

At a glance, it can be observed a decrease in bending moment from 0.03 to 0.04 mm^{-1} curvature. However initially the developed RUC over predicts the bending moment values. As well the stiffness reduction is not that significant as observed by Mallikarachchi et al. [19].

2.4.1 New trend in textile simulation

Recent advancement in computer graphics led to development of tools, which can incorporate complex curved shapes in commercial finite element software packages. Hence, nowadays it is very common and easy task to model the weaved geometry and cross sectional shape of tows in commercially available textile modelling software. TexGen is one of the software that is solely developed for that purpose, to obtain more realistic geometric modelling of textile composites.

There are different methods to represent the yarn path or the weave geometry of a tow. Different studies have various idealization on modelling that. Some studies have adopted a trapezoidal yarn path [30], Some have adopted splines [11], some have adopted sine waves [31]. Cross section was modelled with rectangular shape [10, 11, 30] and sine function [31] Even though most of them were able to capture the stiffness values in geometric linear regime correctly, none were able to accurately predict the non-linear flexural behaviour.

Therefore it is evident that the bending stiffness is dependent on how realistic the geometric parameters are.

Nadarajah et al. [32] compares 3 available yarn path idealization in TexGen, namely linear cubic splines, cubic Bezier splines and natural cubic splines. A comparison on these three methods were carried out by building RUC for two-ply plain weave composite and compared the results in a linear analysis with experimental data. It was revealed that the most suitable modelling scheme would be using of cubic Bezier spline by comparing the results.

Chapter 3

Representative Unit Cell

This chapter encapsulates the idealization process adopted in building the RUC for two-ply plain weave fibre composite laminate encompassing geometric idealization, material properties and generation of the RUC using TexGen textile modelling software [33].

3.1 Identification of Unit Cell

As shown in Figure 2.11 the unit cell of a plain weave lamina can be presented as a repeating geometry. However when there are two laminae involved, the process of identifying RUC will become extremely complicated since there can be infinite number of possibilities of arranging the plies on top of other. Soykasap [10] presented two possible extreme cases of the arrangement called fibre in-phase and fibre out-of phase, Figure 3.1. This study was carried out considering the fibre in-phase case as the base.

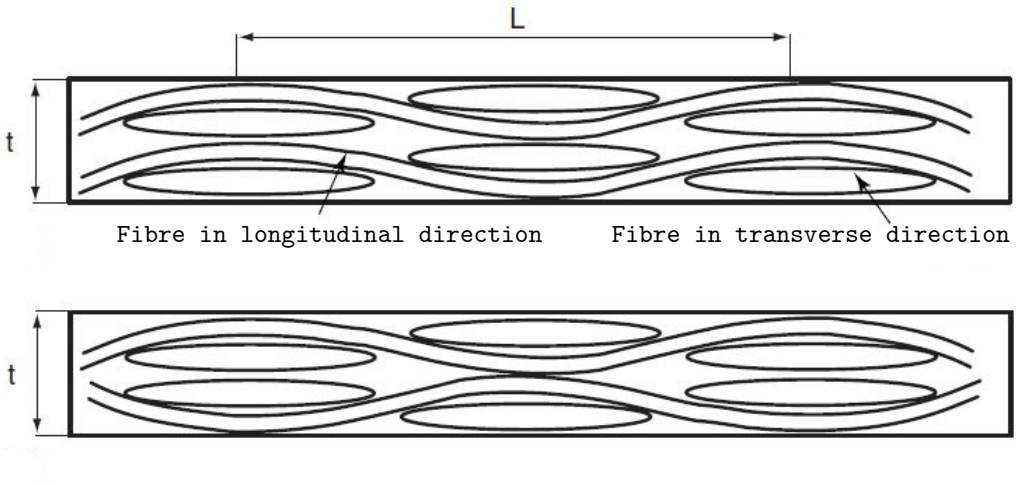

Figure 3.1: Two extreme cases of two-ply arrangement [10]
(a) Fibre in-phase (b) Fibre out-of phase

Then the geometric parameters, i.e. weave length (Δl), tow thickness (a), tow cross sectional area (A), were taken from the previous study done by Mallikarachchi [31], Table 3.1. These parameters were extracted by analysing a series of micrograph, taken from composite made from 1K/T300 carbon fibre and HexPly 913 epoxy resin, Figure 3.2.

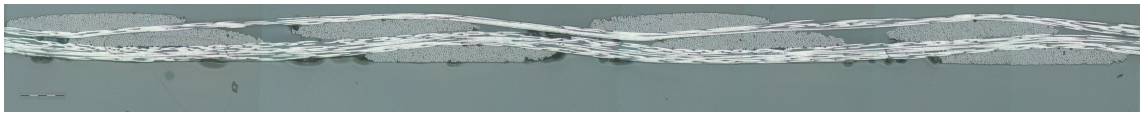

Figure 3.2: Micrograph of 1K T300/913 two-ply plain weave composite [9]

Table 3.1: Geometric properties of 1K T300/913 two-ply plain weave composite [9]

Weave length - Δl (mm)	2.664
Tow thickness - a (mm)	0.059
Cross sectional area - A (mm^2)	0.0522

3.1.1 Geometric Idealization

After obtaining the critical geometric parameters from the literature, tow cross section and weave geometry was idealized. As shown in Figure 3.2, it is not an easy task to incorporate the exact geometry of the tow cross section into the model since it is different from one point to another. This idealization was done by converting it to an ellipse shape which is more realistic than what is been used in the earlier studies, Figure 3.3.

Figure 3.3: Idealization of tow cross-section to an ellipse

When calculating l_1 and l_2, cross sectional area of tow and tow thickness was kept unchanged from the data in Table 3.1. Since those two are the crucial factor for capturing flexural behaviour, Equation 3.1. Hence the two conditions are $A = 0.0522\,\text{mm}^2$ and $l_2 = 0.0295\,\text{mm}$.

$$A = \pi l_1 l_2 \tag{3.1}$$

From the relationship, it was taken $l_1 = 0.561\,\text{mm}$.

3.1.2 Material properties

The composite considered in this study is made out of 1K/T300 carbon fibre from Torayca incorporation and Hexply 913 epoxy resin from Hexply corporation. Since the tows are to be modelled as orthotropic material, material properties should be calculated by considering the effect from both constituents, matrix and fibre. These engineering constants were calculated using the discrete material properties of matrix and fibre and fibre volume fraction (V_f), i.e. ratio of fibre volume to the entire volume of the composite. For this composite, $V_f = 0.62$ [9]. Table 3.2 shows the material properties of two constituents separately.

Table 3.2: Material properties [34, 35]

Properties	**T300 fibre**	**HexPly 913 resin**
Longitudinal stiffness - E_1 (N/mm^2)	233000	3390
Transverse stiffness - E_2 (N/mm^2)	23100	3390
Shear stiffness - G_{12} (N/mm^2)	8963	1210
Poisson's ratio - υ_{12} (N/mm^2)	0.2	0.41
Density - ρ (kg/m^3)	1760	1230
Aerial weight of fabric/film - W (g/mm^2)	98	30

Effective longitudinal stiffness and Poisson's ratio was obtained from the rule of mixtures,

$$E_1 = E_{1f}V_f + E_m(1 - V_f) \tag{3.2}$$

$$\upsilon_{12} = \upsilon_{13} = \upsilon_{12}V_f + \upsilon_m(1 - V_f) \tag{3.3}$$

Transverse stiffness and shear modulus were obtained by Halpin-Tsai equations

$$E_2 = E_3 = E_m\frac{1 + \chi\eta V_f}{1 - \eta V_f} \tag{3.4}$$

where,

$$\eta = \frac{E_{2f} - E_m}{E_{2f} - \chi E_m} \tag{3.5}$$

Here the parameter χ is a measure of reinforcement of the composite, Which was taken as 2 [36].

$$G_{12} = G_{13} = G_m\frac{(G_{12f} + G_m) + V_f(G_{12f} - G_m)}{(G_{12f} + G_m) - V_f(G_{12f} - G_m)} \tag{3.6}$$

Finally in-plane shear modulus, G_{23}, is taken as stated in Quek et al. [37]. Then transverse Poisson's ratio was calculated from Equation 3.7.

$$G_{23} = \frac{E_2}{2(1 + \upsilon_{23})} \tag{3.7}$$

In the idealization process fibre volume fraction (V_f) is taken as 0.62 since all the matrix material is assumed to be included in the tows. This has been done because no additional matrix was modelled in the RUC. With the above techniques, the calculated effective material properties of the tow is presented in Table 3.3.

Table 3.3: Material properties of 1K T300/HexPly 913 tow

Properties	**Value**
Longitudinal stiffness - E_1 (N/mm^2)	145748
Transverse stiffness - $E_2 = E_3$ (N/mm^2)	10427
Shear stiffness - $G_{12} = G_{13}$ (N/mm^2)	3378
In-plane hear stiffness - G_{23} (g/m^2)	3498
Poisson's ratio - $\upsilon_{12} = \upsilon_{13}$	0.28
Poisson's ratio - υ_{23}	0.49

3.2 Building Representative Unit Cell geometry

RUC geometry was generated using the TexGen textile modelling software. Inputted parameters into the TexGen weave module are listed in Table 3.4. Developed geometry for the unit cell is illustrated by Figure 3.4. After obtaining the basic geometry all tows were assigned with the calculated parameters of elliptical geometry in section 3.1.1.

Table 3.4: Entered parameters to TexGen

Tow spacing (half of weave length) (mm)	1.332
Tow width (mm)	1.122
Fabric thickness - t (mm)	0.118

After finishing the geometry, ABAQUS dry fibre file was exported from the TexGen. One drawback of TexGen is, all geometries generated should be meshed in TexGen itself [33] to avoid the incompatibilities occurred in mesh generating algorithms of simulation software, i.e. ABAQUS, and the geometric features generated from TexGen. Therefore the exported .inp (ABAQUS input file) file was generated with a mesh primarily consisting of 3D continuum 8 node

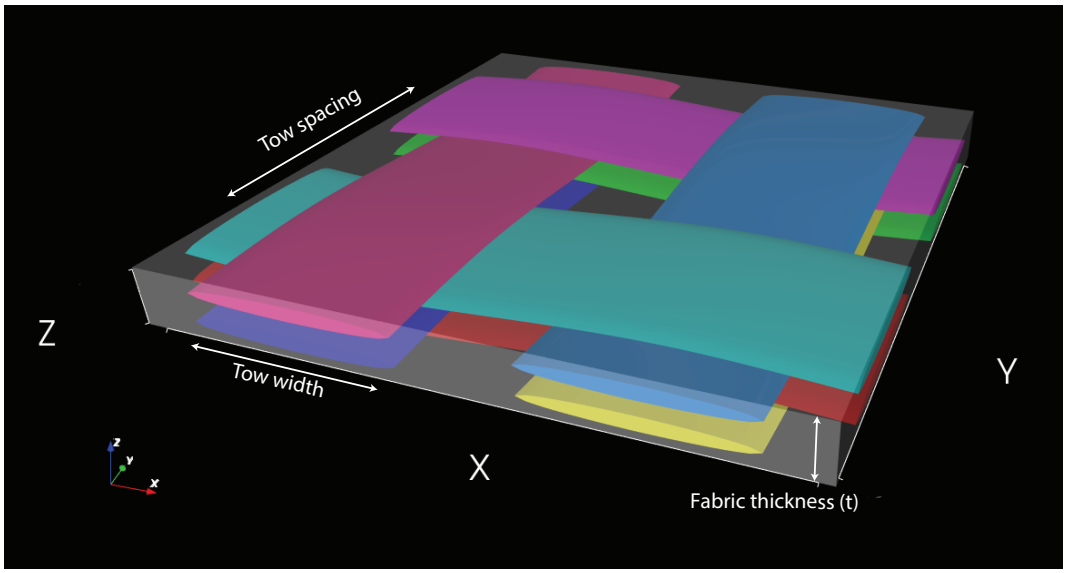

Figure 3.4: Obtained geometry of two-ply plain weave composite from TexGen

linear brick elements with full-integration (C3D8). Another problem of TexGen is that it is not possible to define the element length when exporting the geometry to ABAQUS. Automatically two rows of elements are generated through the thickness of the tow. Hence the element size is heavily varying from element to element due to the elliptical cross sectional shape. However the maximum element size was around 0.05 mm, which is acceptable considering the dimensions of the tow. Finally the model is consisted with 2196 C3D8 elements and 244 six-node wedge elements.

Earlier studies done by Mallikarachchi [31] had a FEA model with six-node wedge elements (C3D6). Therefore the number of integration points through the thickness of a single tow is two at a particular plane of that model. Since the developed model is made of two rows of C3D8 elements per tow. It consists of 4 integration points at a particular plane. Hence it can be deduced that the exported model from TexGen has enough accuracy for the study to continue.

Chapter 4

Predicting Mechanical Properties at Cross-Over Points

This chapter focuses on determining the most suitable interaction of tows at the crossover points and the way that the required properties are extracted. First, it briefs a summary of different behavioural characteristics at the interlacing points and compares the results. Finally the most suitable characteristic was chosen with the hypothetical behaviour and extracted the required mechanical properties through a simulation technique explained thereafter.

4.1 Beahaviour at Cross-Over Points

There are many studies which were focused on the failure of composites in the macro-scale. However almost no research was carried out to describe or predict the behaviour of interlacing points of textile materials. In order to obtain a more realistic numerical model of the RUC, this study has developed a new paradigm based on a hypothesis to extract more accurate behaviour of flexural behaviour.

Most of the past studies have either assumed rigid behaviour in between the tows or simulated the matrix as a deformable body [8, 10, 11, 30, 31]. However, those studies were not successful in capturing the exact flexural behaviour even though the in-plane behaviour was captured correctly.

4.1.1 Rigid connection in-between tows

Soykasap [10] attempted to model the RUC by having kinematic coupling constraints throughout the length of the tow and crossover points as well. Through that, in-plane properties were extracted accurately, but the extracted bending properties did not match with the experimental data even in geometrically linear regime. This deviation was very severe especially for

composites with only 2 to 3 plies.

Unlike in the previous case, Yapa et al. [11] proposed a method to connect only the crossover points with deformable beam connectors, Figure 4.1. That idealization worked fairly well in the geometric linear regime, capturing close values for both bending stiffness and in-plane stiffness.

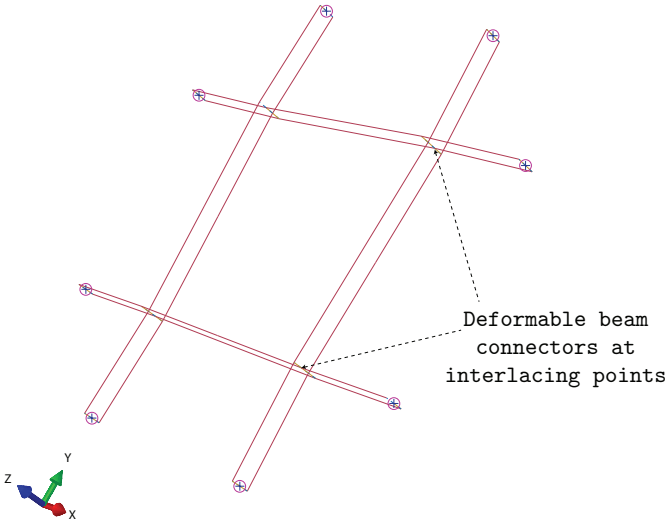

Figure 4.1: 1D RUC with deformable beam connectors at crossover points

Herath et al. [30] built an RUC with rectangular cross section with solid elements and assumed tie constraints at the contact regime of the tows, Figure 4.2. That model has resolved the potential drawback of the 1D RUC described earlier. It represents the actual area contact rather than connecting one single node with the tow in below. Idealization wise 3D solid RUC is way ahead of the beam model.

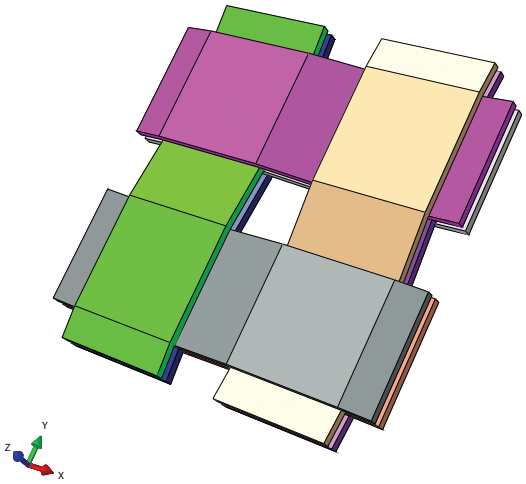

Figure 4.2: 3D solid model with tie constraints at crossover points

4.1.2 Cohesive behaviour in-between tows

Another approach was presuming the adhesive behaviour in between two interlacing tows. This assumption is reasonable by taking the fact that the matrix materilal is actually an adhesive and by that it can be reasonably deduce the cohesive behaviour in between plies. Nadarajah et al. [32] studies the effect of this behaviour by employing cohesive interaction in 3D solid model developed using TexGen, Figure 4.3. Due to lack of the defining of cohesive behaviour, default values of ABAQUS were taken for that particular study which is 1×10^{35} MPa/mm for all the traction values. Ultimately this leads to almost the behaviour of rigid constraint at the contact area.

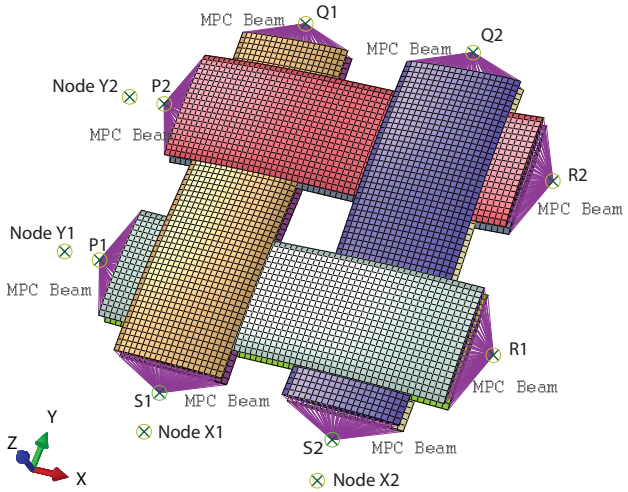

Figure 4.3: 3D solid model with cohesive behaviour at crossover points

4.1.3 Comparison of rigid and cohesive behaviour on RUC

A comparison was conducted between different approaches described earlier, in order to come up with the best behavioural characteristic at interlacing points. For this study, results from Nadarajah et al. [32] and Yapa et al [11] was directly used. RUC from Herath et al. [30] was recreated and 1D beam model with rigid beam connections at crossover points was created too. Figure 4.4 shows the comparison of bending behaviour in non-linear geometric regime.

It can be clearly seen that the there is no variation when the 1D beam element RUC was incorporated with rigid beam connections at the crossover points. Where as both the 3D solid RUC's with tie constraints and cohesive behaviour shows almost same behaviour with the curvature. On both cases

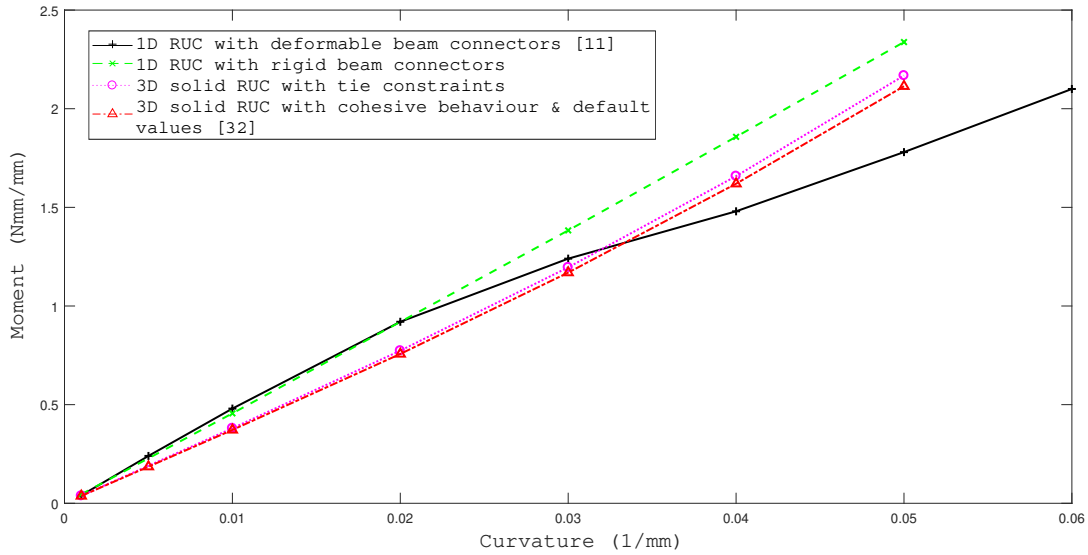

Figure 4.4: Comparison of bending moment vs. curvature graphs for different behavioural conditions [11, 32]

there is a increment in the gradient of graph showing increasing stiffness. In the 1D beam model with deformable beam connections [11], there is slight decrement of bending stiffness from the curvature of 0.02 mm^{-1} to 0.04 mm^{-1}. However, the rest of the parts of the graph is almost flat, having constant bending stiffness value.

From the results, it is evident that idealizing deformable behaviour of the interaction between tows leads to a better prediction on bending stiffness change. Also it can be seen that the effect of modelling reasonable contact area rather than single point matters when capturing the bending stiffness change.

4.2 Developing a New Paradigm

With the evidence from Section 4.1, It upholds that a realistic behaviour of matrix material at the interlacing points are essential when simulating the RUC. So far researchers did not look into the actual effect on epoxy matrix when the composite bends to extremely high curvatures. Hence, this study attempted to develop a new paradigm based on presumed facts and intuitive behavioural characteristics of matrix epoxy.

Even though some researchers attempted to simulate exact behaviour of the

matrix material, none of them were able to do it correctly due to lack of the required data. In 2011, Mallikarachchi [9] stated that one possibility that can describe the bending moment reduction on the two ply plain weave composite through the relative slipping of plies with each other. This slippage involves the cohesiveness of the matrix material and the damage caused to matrix-tow bondage when it yields to high curvatures. A new simulation technique was developed based on that hypothesis in order to simulate the interaction at crossover points, Figure 4.5.

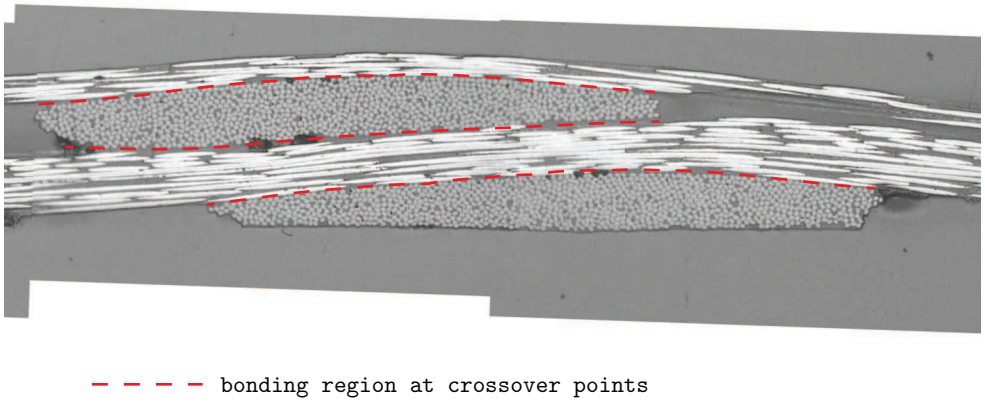

Figure 4.5: Contact regime of perpendicular tows at crossover points

4.2.1 Cohesive behaviour

Cohesive behaviour is used to model the adhesive interface when two or more bodies are connected through an adhesive. Mainly there are two methods to simulate the behaviour of adhesive. First one is by physically modelling the adhesive with cohesive elements and applying the material properties of adhesive to simulate the deformable behaviour. Second approach is defining a cohesive contact interaction between two contact surfaces so the actual cohesive behaviour is modelled virtually. From those two second one is computationally inexpensive compared using cohesive elements. Typically, for a very thin layer of adhesion, cohesive interaction behaviour is used. Since the adhesive thickness is negligible compared to the other dimensions.

Implementation of cohesive interaction behaviour in FEM software

In commercial FEM software, this interaction is defined by relating two

particular nodes in two contact surfaces through a stiffness value. This bonded regime remain bonded throughout the simulation. However unlike in tie constraint this implementation does not constrain rotational degrees of freedoms of the two nodes. These stiffness values are defined through traction separation law. This law is relating the stress in between these two bonded surfaces to the corresponding separation of two bodies. Typically this law depends on the modes of fracture. As there are three basic modes in fracture mechanics. This traction law depends on the all three modes of separation named opening (Mode I), sliding (Mode II), tearing (Mode III). Figure 4.6 shows the three basic modes of fracture.

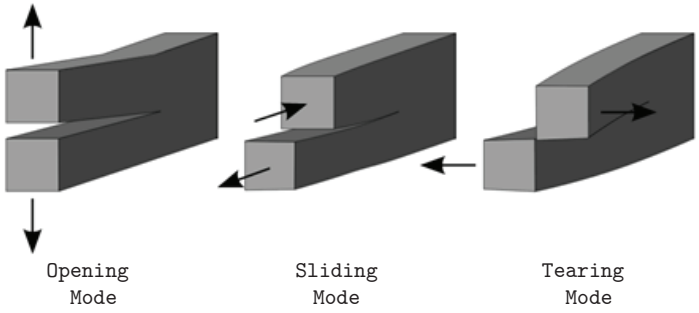

Figure 4.6: Basic modes of fracture

When defining the traction separation law, separation in the direction of Mode I, Mode II & Mode III are denoted by n, s & t respectively. relationship between traction stress vector and separation in three modes can be defined using the 2^{nd} order tensor with traction stiffness values, Equation 4.1

$$\begin{Bmatrix} t_n \\ t_s \\ t_t \end{Bmatrix} = \begin{bmatrix} K_{nn} & K_{ns} & K_{nt} \\ K_{ns} & K_{ss} & K_{st} \\ K_{nt} & K_{st} & K_{tt} \end{bmatrix} \begin{Bmatrix} \delta_n \\ \delta_s \\ \delta_t \end{Bmatrix} \tag{4.1}$$

where, K_{nn}, K_{ss} & K_{tt} are the coupled stiffness values of the three principal directions. For this study the effect of coupling was not considered. So the relationship is reduced as shown by Equation 4.2.

$$\begin{Bmatrix} t_n \\ t_s \\ t_t \end{Bmatrix} = \begin{bmatrix} K_{nn} & 0 & 0 \\ 0 & K_{ss} & 0 \\ 0 & 0 & K_{tt} \end{bmatrix} \begin{Bmatrix} \delta_n \\ \delta_s \\ \delta_t \end{Bmatrix} \tag{4.2}$$

4.2.2 Predicting traction stiffnesses

To define the coupling interaction behaviour K_{nn}, K_{ss} and K_{tt} are needed to feed into the software. However these properties are not readily available through literature. K_{nn} was extracted through a discrete simulation of mode I fracture and the rest of the two stiffness values are derived from that directly since the K_{ss} and K_{tt} are equal for homogeneous and isotropic materials.

To idealize the fracture in normal direction a matrix block with the dimensions of 1 mm × 2 mm × 0.01 mm was chosen and modelled in ABAQUS commercial finite element package, Figure 4.7. Thickness was taken as the element size to minimize the Poisson's effect on the simulation results. 0.5 mm crack over the whole thickness of the block was pre-introduced to the simulation. This tolerates the use of Linear Elastic Fracture Mechanics (LEFM) based XFEM (Extended Finite Element Modelling) method for the simulation.

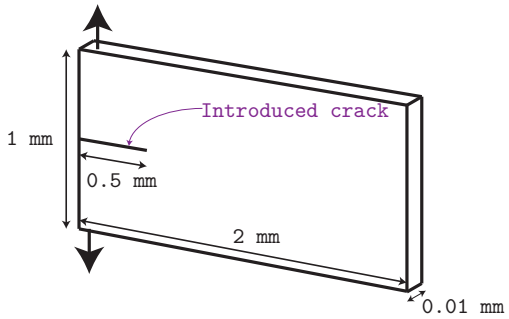

Figure 4.7: Schematic of the matrix block

Basic material properties and tensile strength of the matrix were taken from manufacturer's data stated in Table 3.2. Tensile strength of matrix is 65.5 MPa [34].

After assigning material properties, introduced crack was defined through static XFEM crack modelling technique. Unlike in conventional FEM, XFEM is capable of simulating the initiation and propagation of a discrete crack along an arbitrary, solution-dependent path without the requirement of re-meshing [38]. As shown in Figure 4.7, an arbitrary load was applied to the two faces of the specimen. Then the model was meshed with C3D8 with reduced integration elements consisting 20,000 elements.

Then the model was analysed with ABAQUS/Implicit solver using a server

equipped with Intel Core i9 CPU and 128 GB Ram, utilizing 10 cores and NVIDIA Quadro K2000 General Purpose Graphics Processing Unit (GPGPU) for 8 hours.

Calculation of K_{nn}

Elastic traction stiffness can be evaluated by drawing the displacement and stress at the cohesive zone and calculating the gradient of the graph. For the K_{nn} extraction of opening displacement and normal stresses were done as shown in Figure 4.8 [39].

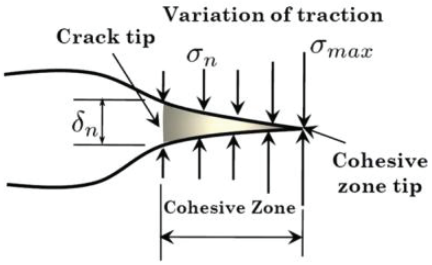

Figure 4.8: Extraction of opening displacement and normal stress at crack tip [39]

Figure 4.9 illustrates the propagated crack in the developed FEM model. Data points were extracted for total of 6 time steps. Normal stress was taken by averaging the stress component in direction 2 (S22) of both the elements adjacent to cohesive zone of the crack. Since the model was meshed with C3D8R elements only one stress value was available in each and every element because it only contains single integration point. These two values were averaged to take the t_n of the cohesive zone. Opening displacement was taken by measuring change of vertical displacement at the end point of initial crack. Table 4.1 summarises the data extracted from the simulation.

Table 4.1: Extracted data from the simulation

Avarage normal stress - t_n (MPa)	**Crack opening (mm)**
0	0
19.84025	7.81662E-05
39.68045	1.56332E-04
59.5207	2.34498E-04
66.5668	2.62259E-04
67.7854	2.67389E-04

Figure 4.10 shows the average normal stress vs crack opening graph for the data extracted. For the data points in the graph a linear trend-line was drawn

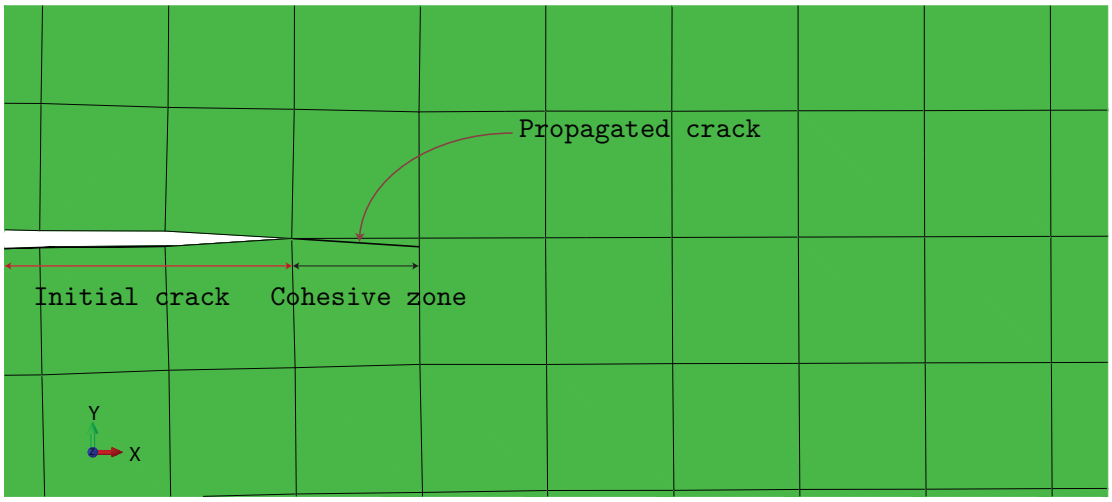

Figure 4.9: Crack propagation of developed simulation

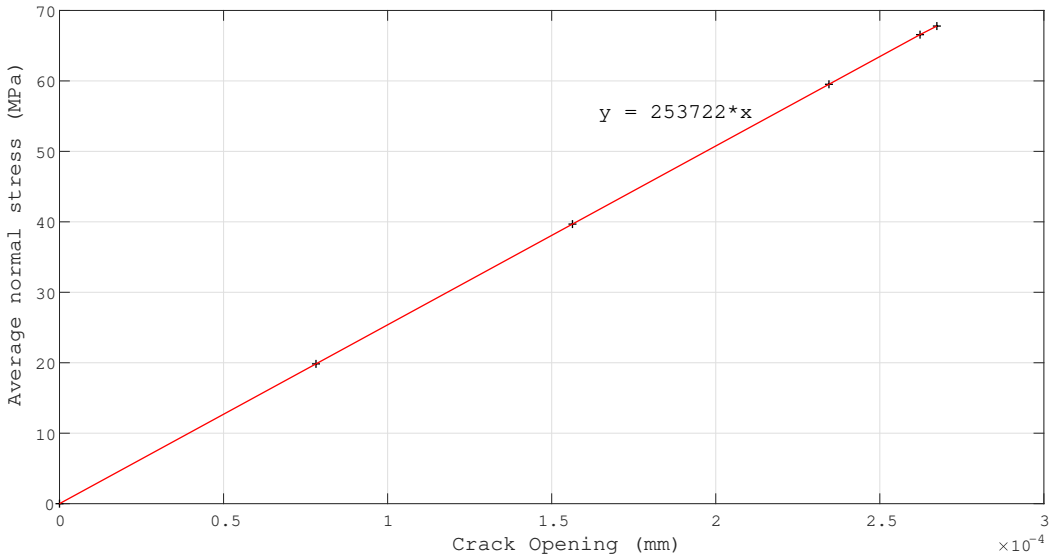

Figure 4.10: Crack opening vs average normal stress

and the gradient was calculated as $253,722$ MPa/mm. As explained earlier this gradient gives the K_{nn} value. From the well known relationship of traction stiffness values, K_{nn} value is directly proportional to the elastic modulus (E) of the material and K_{ss} and K_{tt} are directly proportional to the relevant shear modulus. Since this is the homogeneous and isotropic material $K_{ss} = K_{tt}$. From this relationship both K_{ss} and K_{tt} were calculated as $90,561$ MPa/mm. Table 4.2 summarises the results of traction stiffness values. Units are in MPa/mm.

Table 4.2: Summary of traction stiffness values

Traction stiffness in normal direction (K_{nn})	253722
Traction stiffness in shearing direction (K_{ss})	90561
Traction stiffness in tearing direction (K_{tt})	90561

For the damage modelling, Maximum Principal Stress criterion was selected. Since the matrix material is homogeneous and isotropic, maximum tensile strength can be used to define the failure locus for Maximum Principal Stress criterion.

Chapter 5

Implementation of Unit Cell and Extraction of Results

This chapter presents the steps taken in building the RUC in ABAQUS finite element package with a detailed discussion. Once the FEM models were analysed, relevant displacements and forces were extracted to calculate the ABD matrix using principal of virtual work. Finally the obtained results were discussed by comparing with experimental data presented in Chapter 2.

5.1 Implementing RUC in ABAQUS

As presented in Chapter 3, ABAQUS input file was constructed with the generated geometry from TexGen package. The extracted geometry was then imported to ABAQUS to build the mechanical interaction and analyse the RUC, Figure 5.1. First step of the process was defining the material orientations and the material properties. Material properties were used as calculated in Table 3.3.

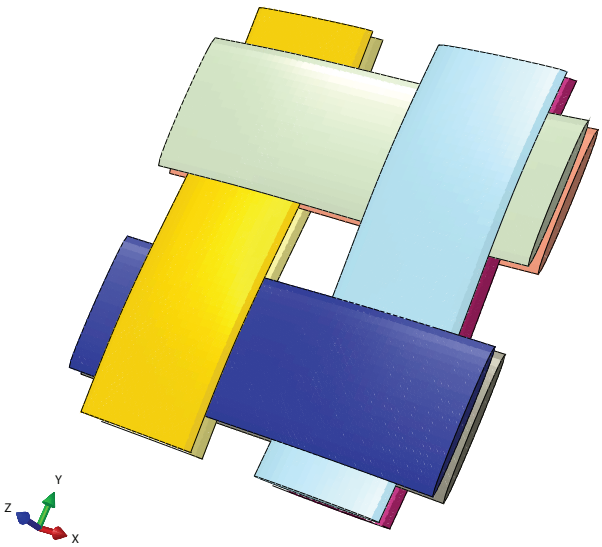

Figure 5.1: Imported model to ABAQUS

5.1.1 Modelling of interlacing points

As presented in Chapter 4 the crossover points are going to be modelled using cohesive interaction modelling. So the adhesive was not modelled with discrete elements. Hence to avoid the nodes that are too much apart from each other, bonding regime was selected as in Figure 5.2. Contact was defined using surface to surface discretisation to avoid the penetration of nodes to the other surface.

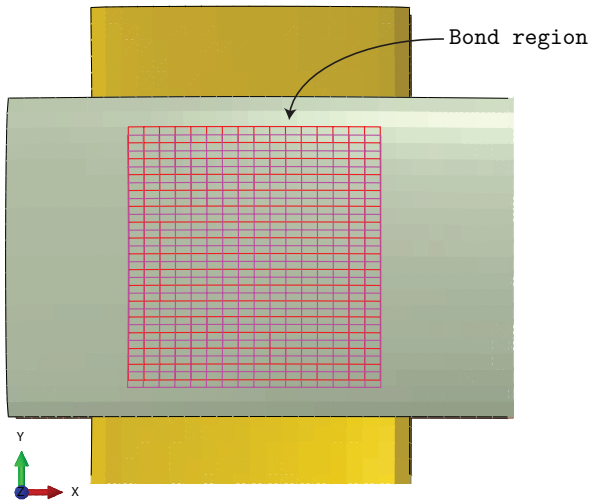

Figure 5.2: Defined contact regime at cross-over points

Cohesive behaviour was assigned using **COHESIVE BEHAVIOUR* keyword and damage properties was assigned by **DAMAGE INITIATION, CRITERION=MAXS* with the Maximum Principal Stress Criterion with the calculated values in Chapter 4.

5.1.2 Homogenized plate model

The developed model was then idealized as a Kirchhoff-Love hypothesis for thin shells to get the constitute relationship as ABD matrix as presented in Chapter 2. The kinematic representation of the said theory is described by the deformation of mid-surface just like Euler-Bernoulli theory for beams as this is based upon that. Relationship of kinematic variables with the mid plane strains are as follows,

$$\varepsilon_x = \frac{\partial u}{\partial x} \tag{5.1}$$

$$\varepsilon_y = \frac{\partial v}{\partial y} \tag{5.2}$$

$$\varepsilon_{xy} = \frac{\partial u}{\partial y} + \frac{\partial v}{\partial x} \tag{5.3}$$

$$\kappa_x = -\frac{\partial^2 w}{\partial x^2} \tag{5.4}$$

$$\kappa_y = -\frac{\partial^2 w}{\partial y^2} \tag{5.5}$$

$$\kappa_{xy} = -2\frac{\partial^2 w}{\partial x \partial y} \tag{5.6}$$

where the x and y are the two in-plane principal directions and u, v and w are displacements in x, y and z directions respectively. It should be noted that the engineering shear strain and twice the surface twist are used to define the shear strain and twisting curvature respectively as in theory of laminated plates [36]. Relationship of the kinematic variables with the respective static variables are shown in Equation 2.4 in the form of ABD matrix.

Periodic boundary conditions

Above explained homogenized plate model was implemented in the developed RUC with the help of PBC. PBC's are often used as a standard tool to represent a large system through the homogenized model. Building of RUC involves exploiting the behaviour of microstructure and modelling the periodicity and symmetries of kinematic variables under loading. Tang and Whitcomb [40] explained this approach in the context of textile composites with assumed displacement fields in unit cell. Karkkainen et al [8] and Kueh and Pellgerino [29] developed this method to incorporate on plain weave and triaxial weave RUCs respectively. This study follows the same approach to implement PBC on the developed micromechanical model. This method involves imposing relative constraints of opposite sides of the RUC. For a homogenized plate model subjected to uniform ϵ and κ, the change in displacement (Δu) and change in rotation ($\Delta\theta$) of two corresponding nodes at opposite boundaries can

be related as follow,

$$\Delta u^x = \varepsilon_x \Delta L \tag{5.7a}$$

$$\Delta v^x = \frac{1}{2}\gamma_{xy} \Delta L \tag{5.7b}$$

$$\Delta u^y = \frac{1}{2}\gamma_{xy} \Delta L \tag{5.7c}$$

$$\Delta v^y = \varepsilon_y \Delta L \tag{5.7d}$$

$$\Delta w^x = -\frac{1}{2}\kappa_{xy} y \Delta L \tag{5.7e}$$

$$\Delta w^y = -\frac{1}{2}\kappa_{xy} x \Delta L \tag{5.7f}$$

$$\Delta \theta_x^x = -\frac{1}{2}\kappa_{xy} \Delta L \tag{5.7g}$$

$$\Delta \theta_y^x = \kappa_x \Delta L \tag{5.7h}$$

$$\Delta \theta_x^y = -\kappa_y \Delta L \tag{5.7i}$$

$$\Delta \theta_y^y = -\frac{1}{2}\kappa_{xy} \Delta L \tag{5.7j}$$

$$\Delta \theta_x^z = 0 \tag{5.7k}$$

$$\Delta \theta_y^z = 0 \tag{5.7l}$$

where subscript denotes the direction of deformation and superscript denotes pair of constraint boundary node. x and y in the equations denotes coordinate of the node pair with respect to relevant X and Y axes respectively.

Figure 5.3 shows the introduced nodes and reference points on the micromechanical model to define the above constraints. First, reference nodes were defined at the mid plane of two plies and connected with each adjacent node in both plies with rigid connectors. This approach was utilized to avoid the formation of rigid plate at the boundary of the tows, although defining single reference node is enough for the calculation. Reference nodes were not defined at the two corner most nodes of the boundary as it over-constraint the deformation since those points only have single node in each tow. 19 reference nodes were introduced per side per couple of tow, totalling 152 altogether covering four sides. 72 dummy nodes were introduced to relate the kinematic variable of a reference node with the particular reference node on the opposite side. It sums up to 72 pairs of reference nodes and each set has to be constrained on all 6 degrees of freedom as in Equation 5.7a to 5.7l.

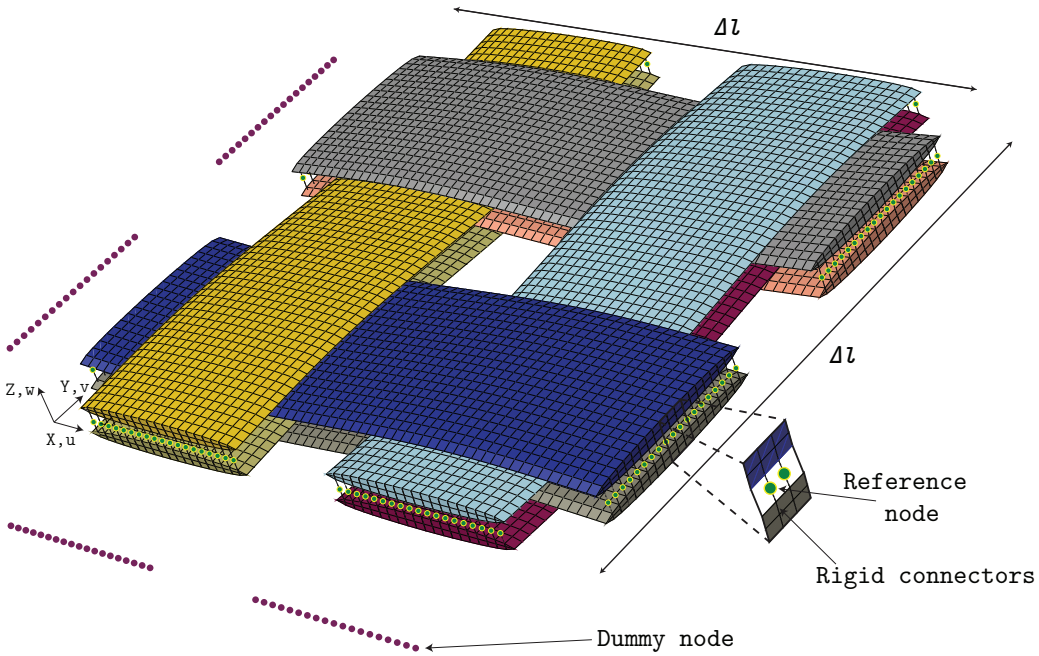

Figure 5.3: Developed RUC

The constraints were defined in ABAQUS using **EQUATION* command. Considering the large number of equations involved, a Python scrip was written to pre-processing of equation constraints, Annex A.1. Then the generated equations were included in the ABAQUS input file.

5.2 Calculating ABD Matrix

Six separate analyses were done imposing six unit deformation modes on the RUC. Every mode was analysed by setting one average strain/curvature to one (or any other value in non-linear analysis) and all others equal to zero. For an example, in the first linear analysis, $\epsilon_{xx} = 1$ while $\epsilon_{yy} = \epsilon_{xy} = 0$ and $\kappa_{xx} = \kappa_{yy} = \kappa_{xy} = 0$. All six deformation modes for one typical strain/curvature is presented in Figure 5.4. These deformation modes were imposed by using the **BOUNDARY* command in ABAQUS. Likewise all six deformation modes were analysed. Then the displacements and rotations of dummy nodes and corresponding forces and moments of reference nodes were extracted for the computation of ADB matrix.

5.2.1 Principal of virtual work

Principal of virtual work was used to calculate the entries of the ABD matrix. Equation 5.8 shows relationship of the work done by the force resultant in the

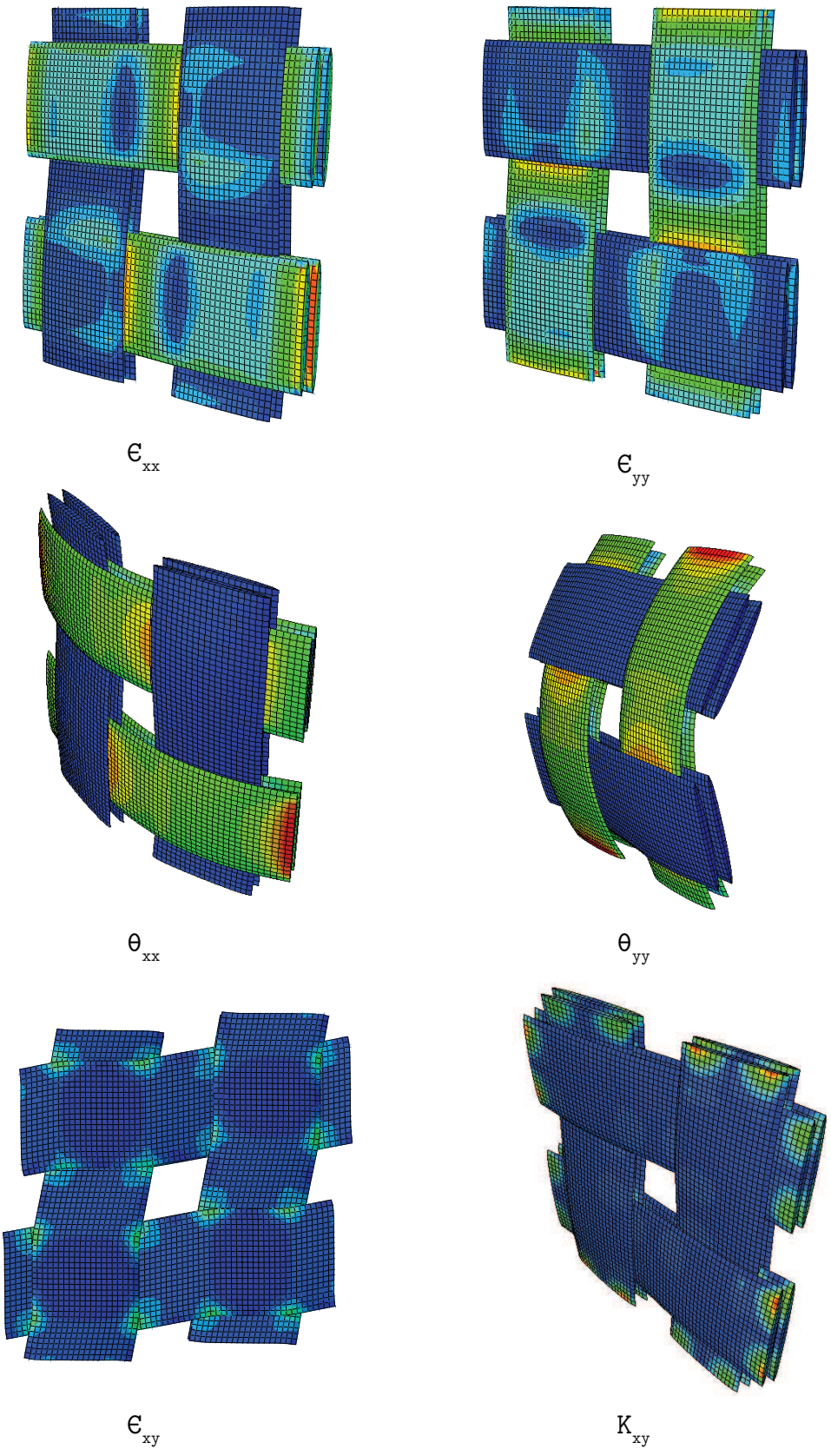

Figure 5.4: Six deformation modes for a typical analysis

direction of X axis and by individual dummy nodes in the first deformation mode, i.e. $\epsilon_{xx} \neq 0$.

$$N_{xx}\epsilon_{xx}\Delta l^2 = \sum_{d.n.}(F_x u + F_y v + F_z w + M_x\theta + M_y\theta + M_z\theta) \tag{5.8}$$

where the summation is extended to all 152 dummy nodes. After substituting $A_{11}\epsilon_{xx} = N_{xx}$, Equation 5.9 gives the value to A_{11}.

$$A_{11} = \frac{\sum_{d.n.}(F_x u + F_y v + F_z w + M_x\theta + M_y\theta + M_z\theta)}{\epsilon_{xx}^2\Delta l^2} \tag{5.9}$$

Likewise, all other entries of the ABD matrix can be calculated through the same principal.

5.2.2 Extraction and processing of data

Considering the number of reference nodes and dummy nodes involved forces, moments, displacement and rotations were written to the data file using **NODE PRINT* command in ABAQUS. The data request command lines were generated through a Python script, (Annex A.2), and included in the ABAQUS input file.

Due to the high number of nodes involved, the calculation of ABD matrix was done by setting up two matrices with 912 rows (with 6 degrees of freedom per node times 152 dummy nodes) and 6 columns for six deformation modes.

First matrix (U) contains the kinematic variables (i.e. displacements and rotations) of dummy nodes for each deformation mode which were directly extracted from ABAQUS data file. Second matrix (F) contains the forces and moments of dummy nodes for each deformation mode which was calculated from the extracted forces and moments at reference nodes. Finally the ABD matrix can be calculated by the following Equation 5.10. Processing of data was carried out by a MATLAB script developed in this study, Appendix C.

$$ABD = \frac{U^T F}{\Delta l_x^2} \tag{5.10}$$

It should be noted that the above Equation 5.10 is only valid for linear analysis where all the strain/curvature values are unit. In the non-linear analysis expression should be divided by square of the relevant strain/curvature introduced in the deformation modes.

5.3 Results and Discussion

ABD matrices were extracted for linear analysis and considering the non linear geometric effect separately. In the non-linear regime 6 analyses were carried out to obtain ABD matrix for strain/curvature of 0.001, 0.005, 0.01, 0.02, 0.03. These results were compared with the experimental data presented in Section 2.1.2.

5.3.1 Linear analysis

Extracted ABD matrix for the linear analysis is shown below, Equation 5.11.

$$ABD = \left[\begin{array}{ccc|ccc} 8017 & 1403 & 0 & 0 & 0 & 1 \\ 1403 & 8016 & 0 & 0 & 0 & 1 \\ 0 & 0 & 198 & 0 & 0 & 0 \\ \cdots & \cdots & \cdots & \cdots & \cdots & \cdots \\ 0 & 0 & 0 & 37.3 & 0.5 & 0 \\ 0 & 0 & 0 & 0.5 & 37.4 & 0 \\ 1 & 1 & 0 & 0 & 0 & 1.4 \end{array}\right] \tag{5.11}$$

This was compared with experimental results from Mallikarachchi [31]. Since the testing was done using long narrow specimens, transverse and shear stress resultants can be considered as negligible. Compliance of A submatrix denoting by a_{ij} was calculated and then $1/a_{11}$ can be compared with the results from the tensile test. Experimental results from four point bending test can be directly compared with D_{11}. Table 5.1 shows a summary of the results from the developed simulation technique and experiments carried out by Mallikarachchi [31]. It can be clearly seen from the results that the developed simulation method is capable of capturing the initial flexural behaviour with a good accuracy.

Table 5.1: Comparison of material properties obtained for two-ply plain weave 1K-T300/913

Property	**Simulation**	**Experiment [31]**
Bending stiffness - D_{11} (Nmm)	37.3	37.55 ± 5.54
Poisson's ratio - v_{12}	0.18	0.11 ± 0.03

5.3.2 Geometric non-linear analysis

Figure 5.5 presents extracted results for beam model with rigid connectors at cross-over points, solid model with rectangular cross section with tie constraints at cross-over points, solid model generated by TexGen with cohesive behaviour at the cross-over points and solid model generated by TexGen with cohesive and damage behaviour at the cross-over points. Beam model does not show any variation of bending stiffness with the curvature whereas other two with tie constraints and cohesion only behaviour are possessing an increment in bending stiffness. Hence it is evident that these methods are not viable on capturing the bending stiffness variation successfully.

Since the developed RUC with cohesive and damage behaviour accurately captured the initial bending stiffness, simulations were extended to geometric non-linear analysis. ABD matrices were calculated for strain/curvature values of 0.001, 0.005, 0.01, 0.02, 0.03 to observe the behaviour of the bending stiffness over the curvature. As shown in Figure 5.5, it was able to capture a reduction in bending stiffness with increasing curvature successfully.

Further analysis could not be able to run after reaching 0.03 curvature point due to numerical difficulties as the minimum allowable time step of 1×10^{-35} has been reached. Typical analysis took around an hour to complete on a consumer grade laptop utilizing 4 cores and 8 GB of RAM memory.

Hence the extracted D_{11} values for each case were plotted in a graph, then it was extrapolated till the failure curvature using a cubic interpolating function of the available data points from simulation and the average failure point from platen folding test conducted by Mallikarachchi [31]. Figure 5.6 illustrates the summary of the obtained results and the experimental data. In order to predict the bending behaviour till the failure, a point near the failure is required to extrapolate the function. Since a failure test is a must to build the failure

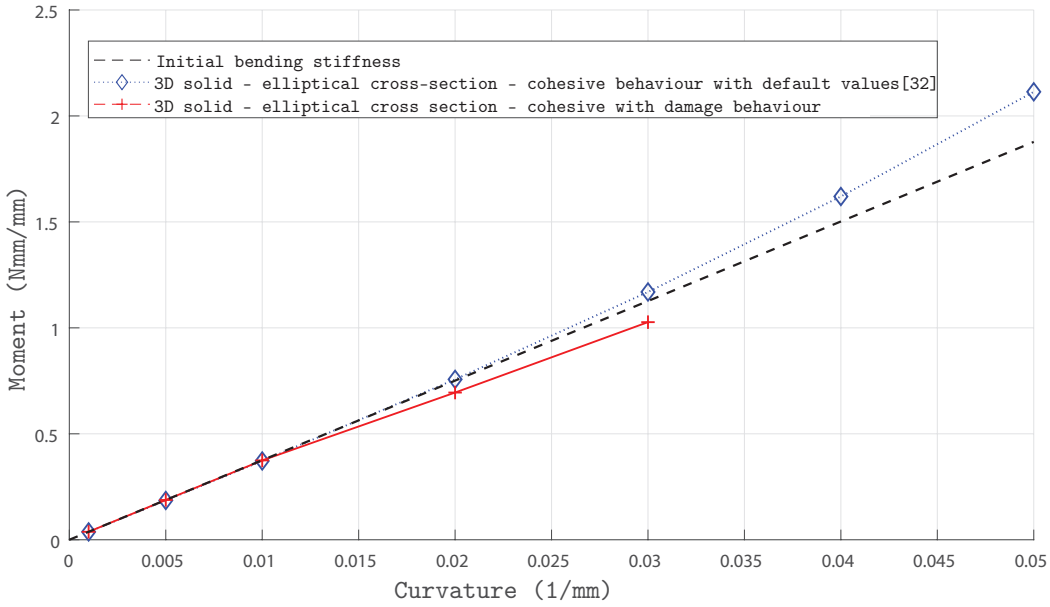

Figure 5.5: Comparison of bending moment vs. curvature with adhesive behaviour

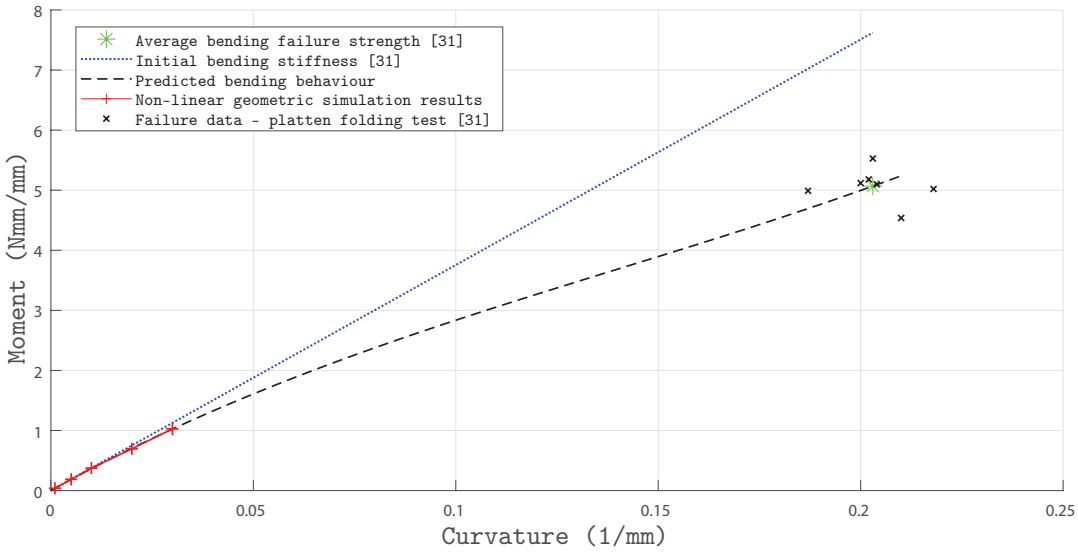

Figure 5.6: Comparison of predicted bending behaviour with experimental data

criterion for the optimization purposes, getting the bending moment near the failure curvature is not an additional burden.

Unlike the previous studies, developed method is capable of predicting reduction in bending stiffness with increasing curvature.

Chapter 6

Conclusions and Future Work

6.1 Conclusions

Understanding flexural behaviour of thin woven fibre composites is a crucial in designing weight sensitive structures. The reduction of bending stiffness with high curvatures was a long standing question. Even though people have observed this behaviour in physical testing, a feasible explanation for this behaviour was not presented earlier; being a bottleneck for utilizing simulations in the design process. This study has presented a paradigm for this particular behaviour and proved the effectiveness of it through virtual simulations.

One of the crucial parts of micromechanical models is idealizing the geometry of the actual microstructure without compromising the behavioural characteristics. Past studies were limited to crude idealization techniques when it comes to defining weave geometry and cross section profile. In this study, more realistic geometry was developed through a well established textile geometry modelling software. Cross section was idealized as an elliptical shape and cubic Bezier splines were used to define the weave geometry of two-ply plain weave 1K-T300/913 composite.

Another important factor of developing RUC for woven composites is the interaction of tows at the crossover points. It was not clear the behaviour of the epoxy matrix under high curvatures. Previously researchers have utilized different methods to idealize interactive behaviour at these tow interlacing points by means of rigid connections and modelling deformable body. This thesis presents a new paradigm for the behaviour of the matrix material at those points and successfully utilized it in a micromechanical model.

The new logical framework taken into account the possibility of relative

slipping and damage initiation at the interlacing points under high curvatures. This behaviour can be characterised using the traction separation law and damage criteria. Even though present day commercial FEA software are capable of handling these complex scenarios, lack of a reliable method to predict material properties was a huge barrier on simulating this behaviour. As a counteract for the problem, a new method was proposed to extract the required material properties from discrete virtual simulation of matrix material.

The proposed method to extract the traction coefficients involves simulating the fracturing of matrix. Through that a relationship of stress state and displacement at the cohesive zone of the crack (i.e. crack tip) was developed in the normal direction. Afterwards the normal traction coefficient K_{nn} was calculated by the gradient of the plotted graph and other two coefficients in shearing and tearing direction were taken by material definition. Maximum principal stress criterion was used as the damage initiating criterion at the contact regime of the tows.

Proposed strategy was imposed in the developed geometric model of the RUC and the simulations were carried out. Flexural behaviour at linear regime was captured with great accuracy, although there were disparities in extensional stiffness and Poisson's ratio. With the close agreement of bending stiffness result for the linear regime, analysis was further extended to non-linear geometric regime. Simulations were not able to complete after 0.03 curvature due to numerical difficulties. However function was extrapolated till the failure point using the extracted simulation results and the data points from platen folding experiments. Predicted function shows a bending stiffness reduction till the failure which was not been able to capture with the past studies. Nevertheless, the accuracy of the developed simulation technique should be verified with an experiment before implementing it in the design process of booms.

The proposed strategy with the traction-coefficient determined from virtual testing can be utilized in the development of deployable booms made out of thin woven fibre composites through multi-scale modelling. Even though the building of this particular simulation was time consuming and involves many steps, most of the work can be automated through the use of Python and MATLAB as explained in the main body. Nevertheless, it should be noted that the proposed

simulation technique was developed based on several assumptions, namely; coupling of traction stiffnesses and the effect from the texture of the fabric on traction stiffness was disregarded, as well there are several assumptions taken in extracting stress and displacement field on the crack tip as explained earlier.

6.2 Future Work

The following are some suggested future research directions.

1. Further development of proposed simulation technique to capture the bending behaviour near failure point to avoid extrapolation.

2. Verification of the proposed method for the extraction of traction coefficients through experiments.

References

[1] C. Soutis, "Fibre reinforced composites in aircraft construction," *Progress in Aerospace Sciences*, vol. 41, no. 2, pp. 143–151, Feb. 2005.

[2] R. Jordan, G. Picardi, J. Plaut, K. Wheeler, D. Kirchner, A. Safaeinili, W. Johnson, R. Seu, D. Calabrese, E. Zampolini, A. Cicchetti, R. Huff, D. Gurnett, A. Ivanov, W. Kofman, R. Orosei, T. Thompson, P. Edenhofer, and O. Bombaci, "The mars express marsis sounder instrument," *Planetary and Space Science*, vol. 57, no. 14-15, pp. 1975–1986, Dec. 2009.

[3] O. Soykasap, "Deployment analysis of a self-deployable composite boom," *Composite Structures*, vol. 89, no. 3, pp. 374–381, Jul. 2009.

[4] H. Mallikarachchi and S. Pellegrino, "Deployment dynamics of composite booms with integral slotted hinges," in *in Collection of Technical Papers - AIAA/ASME/ASCE/AHS/ASC Structures, Structural Dynamics and Materials Conference*. American Institute of Aeronautics and Astronautics, 2009.

[5] S. Timoshenko, *Theory of Plates and Shells*, 2nd ed. McGraw-Hill Book Company, 1987.

[6] B. Le Page, F. Guild, S. Ogin, and P. Smith, "Finite element simulation of woven fabric composites," *Composites Part A: Applied Science and Manufacturing*, vol. 35, no. 7-8, pp. 861–872, Jul. 2004.

[7] R. A. Naik, "Failure analysis of woven and braided fabric reinforced composites," *Journal of Composite Materials*, vol. 29, no. 17, pp. 2334–2363, Nov. 1995.

[8] R. Karkkainen and B. Sankar, "A direct micromechanics method for analysis

of failure initiation of plain weave textile composites," *Composites Science and Technology*, vol. 66, no. 1, pp. 137–150, Jan. 2006.

[9] H. Mallikarachchi, "Thin-walled composite deployable booms with tape-spring hinges," PhD thesis, University of Cambridge, May 2011.

[10] O. Soykasap, "Micromechanical models for bending behavior of woven composites," *Journal of Spacecraft and Rockets*, vol. 43, no. 5, pp. 1093–1100, Sep. 2006.

[11] Y. Yapa and H. Mallikarachchi, "Predicting non-linear bending behaviour of thin woven fibre composites," in *Society of Structural Engineers, Sri Lanka - Annual Sessions 2017*. SSESL, Aug. 2017.

[12] M. Mikula and M. Thomson, "Large space structures (state-of-the-art and technology needs)," in *33rd Structures, Structural Dynamics and Materials Conference*, Apr. 1992.

[13] W. Wuest, "Some applications of the theory of the cylindrical shell," *Journal of Applied Mathematics and Mechanics*, Nov. 1953.

[14] O. Soykasap, "Analysis of tape spring hinges," *International Journal of Mechanical Sciences*, Jan. 2007.

[15] K. Seffen and S. Pellegrino, "Deployment dynamics of tape springs," in *Proceedings of The Royal Society A*, Mar. 1999.

[16] W. Vyvyan, "Self-actuating, self-locking hinge," USA patentus 3 386 128, Jun., 1968.

[17] K. Ubamanyu, "Simulation of closed cross section dual matrix composite booms," MSc thesis, University of Moratuwa, Aug. 2017.

[18] M. Sakovsky, "Design and characterization of dual-matrix composite deployable space structures," PhD thesis, California Institute of Technology, May 2018.

[19] H. Mallikarachchi and S. Pellegrino, "Failure criterion for two-ply plain-weave cfrp laminates," *Journal of Composite Material*, vol. 47, no. 11, Sep. 2012.

[20] G. Sanford and A. Biskner, "Large strain behavior of thin unidirectional composite flexures," in *51st AIAA/ASME/ASCE/AHS/ASC Structures, Structural Dynamics, and Materials Conference*. AIAA, Apr. 2010.

[21] R. M. Jones, *Mechanics of Composite Material*, second edition ed. Taylor & Francis Inc., 1999.

[22] M. F. Horstemeyer, *Integrated Computational Materials Engineering (ICME) for Metals: Using Multiscale Modeling to Invigorate Engineering Design with Science*. John Wiley & Sons, Inc., 2012.

[23] B. E. Said, F. Daghia, D. Ivanov, and S. R. Hallett, "An iterative multiscale modelling approach for nonlinear analysis of 3d composites," *International Journal of Solids and Structures*, vol. 132-133, pp. 42–58, Feb. 2018.

[24] A. D. B. Ferreira, P. R. Nvoa, and A. T. Marques, "Multifunctional material systems: A state-of-the-art review," *Composite Structures*, vol. 151, pp. 3 – 35, 2016, smart composites and composite structures In honour of the 70th anniversary of Professor Carlos Alberto Mota Soares. [Online]. Available: http://www.sciencedirect.com/science/article/pii/S0263822316000416

[25] T. Ishikawa and T.-W. Chou, "Elastic behavior of woven hybrid composites," *Journal of Composite Materials*, vol. 16, no. 1, pp. 2–19, Jan. 1982.

[26] T. Ishikawa and T.-W. Chou, "One-dimensional micromechanical analysis of woven fibre composites," *AIAA Journal*, vol. 21, pp. 1714–1721, 1983.

[27] B. Cox, W. Carter, and F. N.A., "A binary model of textile composites - i formulation," *Acta Metallurgica et Materialia*, vol. 42, no. 10, pp. 3463–3479, Oct. 1994.

[28] M. McGlockton, B. Cox, and R. McMeeking, "A binary model of textile composites - iii high failure strain and work of fracture in 3d weaves," *Journal of the Mechanics and Physics of Solids*, vol. 51, no. 8, Aug. 2003.

[29] A. Kueh and S. Pellegrino, "Abd matrix of single-ply triaxial weave fabric composites," in *48th AIAA/ASME/ASCE/AHS/ASC Structures, Structural Dynamics, and Materials Conference*, Apr. 2007.

[30] H. Herath and H. Mallikarachchi, "Modified ply thickness for classical lamination theory for thin woven fibre composites," in *Annual Sessions of Institution of Engineers Sri Lanka -2016*. IESL, Oct. 2016.

[31] H. Mallikarachchi, "Predicting mechanical properties of thin woven carbon fiber reinforced laminates," *Thin-Walled Structures*, vol. 135, pp. 297–305, Feb. 2019.

[32] S. Nadarajah, M. Jayasekara, and H. Mallikarachchi, "Non-linear bending response of two-ply plain woven carbon fibre composites," in *5th Moratuwa Engineering Research Conference (MERCon) - 2019*. Engineering Research Unit, University of Moratuwa, 2019.

[33] TexGen, "TexGen Userguide," University of Nottingham Textile Composites Research Group, Nottingham, UK, 2019.

[34] Hexcel, "Technical Data Sheet HexPly913,Hexcel Composites," Hexcel Corporation, Stamford, Connecticut, United States, 2007.

[35] Toray, "Technical data sheet no. cfa-001, t300 data sheet," Toray Industries, Ch, Tokyo, Japan, 2007.

[36] M. Daniel and O. Ishai, *Engineering Mechanics of Composite Materials*, 2nd ed. McGraw-Hill Book Company, 2006.

[37] S. C. Quek, A. M. Waas, K. W. Shahwan, and V. Agaram, "Analysis of 2d triaxial flat braided textile composites," *International Journal of Mechanical Sciences*, vol. 45, no. 6, pp. 1077 – 1096, 2003. [Online]. Available: http://www.sciencedirect.com/science/article/pii/S0020740303001632

[38] T. Belytschko and T. Black, "Elastic crack growth in finite elements with minimal remeshing," *International Journal for Numerical Methods in Engineering*, vol. 45, pp. 601 – 620, May 1999.

[39] C. K. Desai, S. Basu, and V. Parameswaran, "Determination of traction separation law for interfacial failure in adhesive joints at different loading rates," *The Journal of Adhesion*, vol. 92, no. 10, pp. 819 – 839, May 2015.

[40] X. Tang and J. D. Whitcomb, "General techniques for exploiting periodicity and symmetries in micromechanics analysis of textile composites," *Journal of Composite Materials*, vol. 37, no. 13, pp. 1167–1189, 2003. [Online]. Available: https://doi.org/10.1177/0021998303037013003

Appendix A

Python Scripts for Pre-Processing

A.1 Generating Equation Constraints

```
-----------------------------------------------------------------------
** Reading X coefficients of S1 node set
-----------------------------------------------------------------------
fo_S1 = open('./S1.txt', "r+")
lines_S1 = fo_S1.readlines()
fo_S1.close()
#print (lines_S1)

n = 1
coef_S1 = list();

while (n<22):
    coef_S1.append(1)
    coef_S1[n-1] = float(lines_S1[n-1])
    n += 1
-----------------------------------------------------------------------
** Reading X coefficients of S2 node set
-----------------------------------------------------------------------
.................
.................
-----------------------------------------------------------------------
** Reading Y coefficients of P2 node set
-----------------------------------------------------------------------
fo_P2 = open('./P2.txt', "r+")
```

```
lines_P2 = fo_P2.readlines()
fo_P2.close()
#print (lines_P2)

n = 1
coef_P2 = list();

while (n<22):
    coef_P2.append(1)
    coef_P2[n-1] = float(lines_P2[n-1])
    n += 1
```

```
** Writing equation set for Q1S1\\
```

```
fo_Q1S1 = open('./Q1S1.txt', "w+")
length = 2.658
ni = 1

while (ni<22):
    coefficient = float(coef_S1[ni-1]*length)
    fo_Q1S1.write("** Constraint: Q1-%d_S1-%d_RXy \n"
    % (ni, ni))
    fo_Q1S1.write("*Equation \n")
    fo_Q1S1.write("3 \n")
    fo_Q1S1.write("Q1-%d, 4, 1. \n" % (ni))
    fo_Q1S1.write("S1-%d, 4, -1. \n" % (ni))
    fo_Q1S1.write("Node_X1-%d, 4, 2.658 \n" % (ni))
    fo_Q1S1.write("** Constraint: Q1-%d_S1-%d_RYy \n"
    % (ni, ni))
    fo_Q1S1.write("*Equation \n")
    fo_Q1S1.write("3 \n")
    fo_Q1S1.write("Q1-%d, 5, 1. \n" % (ni))
    fo_Q1S1.write("S1-%d, 5, -1. \n" % (ni))
    fo_Q1S1.write("Node_X1-%d, 5, -2.658 \n" % (ni))
    fo_Q1S1.write("** Constraint: Q1-%d_S1-%d_RZy \n"
    % (ni, ni))
```

```
    fo_Q1S1.write("*Equation \n")
    fo_Q1S1.write("3 \n")
    fo_Q1S1.write("Q1-%d, 6, 1. \n" % (ni))
    fo_Q1S1.write("S1-%d, 6, -1. \n" % (ni))
    fo_Q1S1.write("Node_X1-%d, 6, 0. \n" % (ni))
    fo_Q1S1.write("** Constraint: Q1-%d_S1-%d_Uy \n"
    % (ni, ni))
    fo_Q1S1.write("*Equation \n")
    fo_Q1S1.write("3 \n")
    fo_Q1S1.write("Q1-%d, 1, 1. \n" % (ni))
    fo_Q1S1.write("S1-%d, 1, -1. \n" % (ni))
    fo_Q1S1.write("Node_X1-%d, 1, -2.658 \n" % (ni))
    fo_Q1S1.write("** Constraint: Q1-%d_S1-%d_Vy \n"
    % (ni, ni))
    fo_Q1S1.write("*Equation \n")
    fo_Q1S1.write("3 \n")
    fo_Q1S1.write("Q1-%d, 2, 1. \n" % (ni))
    fo_Q1S1.write("S1-%d, 2, -1. \n" % (ni))
    fo_Q1S1.write("Node_X1-%d, 2, -2.658 \n" % (ni))
    fo_Q1S1.write("** Constraint: Q1-%d_S1-%d_Zy \n"
    % (ni, ni))
    fo_Q1S1.write("*Equation \n")
    fo_Q1S1.write("3 \n")
    fo_Q1S1.write("Q1-%d, 3, 1. \n" % (ni))
    fo_Q1S1.write("S1-%d, 3, -1. \n" % (ni))
    fo_Q1S1.write("Node_X1-%d, 3, %f \n"
    % (ni,coefficient))
    ni += 1

fo_Q1S1.close()
.................
.................
```

```
** Writing equation set for R2P2
```

```
fo_R2P2 = open('./R2P2.txt', "w+")
ni = 1

while (ni<22):
    coefficient = float(coef_P2[ni-1]*length)
    fo_R2P2.write("** Constraint: R2-%d_P2-%d_RXx \n"
    % (ni, ni))
    fo_R2P2.write("*Equation \n")
    fo_R2P2.write("3 \n")
    fo_R2P2.write("R2-%d, 4, 1. \n" % (ni))
    fo_R2P2.write("P2-%d, 4, -1. \n" % (ni))
    fo_R2P2.write("Node_Y2-%d, 4, 2.658 \n" % (ni))
    fo_R2P2.write("** Constraint: R2-%d_P2-%d_RYx \n"
    % (ni, ni))
    fo_R2P2.write("*Equation \n")
    fo_R2P2.write("3 \n")
    fo_R2P2.write("R2-%d, 5, 1. \n" % (ni))
    fo_R2P2.write("P2-%d, 5, -1. \n" % (ni))
    fo_R2P2.write("Node_Y2-%d, 5, -2.658 \n" % (ni))
    fo_R2P2.write("** Constraint: R2-%d_P2-%d_RZx \n"
    % (ni, ni))
    fo_R2P2.write("*Equation \n")
    fo_R2P2.write("3 \n")
    fo_R2P2.write("R2-%d, 6, 1. \n" % (ni))
    fo_R2P2.write("P2-%d, 6, -1. \n" % (ni))
    fo_R2P2.write("Node_Y2-%d, 6, 0. \n" % (ni))
    fo_R2P2.write("** Constraint: R2-%d_P2-%d_Ux \n"
    % (ni, ni))
    fo_R2P2.write("*Equation \n")
    fo_R2P2.write("3 \n")
    fo_R2P2.write("R2-%d, 1, 1. \n" % (ni))
    fo_R2P2.write("P2-%d, 1, -1. \n" % (ni))
    fo_R2P2.write("Node_Y2-%d, 1, -2.658 \n" % (ni))
    fo_R2P2.write("** Constraint: R2-%d_P2-%d_Vx \n"
    % (ni, ni))
    fo_R2P2.write("*Equation \n")
```

```
    fo_R2P2.write("3 \n")
    fo_R2P2.write("R2-%d, 2, 1. \n" % (ni))
    fo_R2P2.write("P2-%d, 2, -1. \n" % (ni))
    fo_R2P2.write("Node_Y2-%d, 2, -2.658 \n" % (ni))
    fo_R2P2.write("** Constraint: R2-%d_P2-%d_Zx \n"
    % (ni, ni))
    fo_R2P2.write("*Equation \n")
    fo_R2P2.write("3 \n")
    fo_R2P2.write("R2-%d, 3, 1. \n" % (ni))
    fo_R2P2.write("P2-%d, 3, -1. \n" % (ni))
    fo_R2P2.write("Node_Y2-%d, 3, %f \n"
    % (ni,coefficient))
    ni += 1

fo_R2P2.close()
```

A.2 Generating Data Request Command-Lines

```
-------------------------------------------------------------

# Output request lines for dummy nodes

-------------------------------------------------------------

fo_out = open('./output request lines.txt', "w+")

ni = 1

while (ni<22):
    fo_out.write("*Node Print, Nset=Node_Y1-%d,
    Summary=No, freq=1 \n" % (ni))
    fo_out.write("RF \n")
    fo_out.write("*Node Print, Nset=Node_Y2-%d,
    Summary=No, freq=1 \n" % (ni))
    fo_out.write("RF \n")
    fo_out.write("*Node Print, Nset=Node_X1-%d,
    Summary=No, freq=1 \n" % (ni))
    fo_out.write("RF \n")
    fo_out.write("*Node Print, Nset=Node_X2-%d,
    Summary=No, freq=1 \n" % (ni))
```

```
    fo_out.write("RF \n")
    ni += 1

#-------------------------------------------------------------------------
# Output request lines for reference nodes
#-------------------------------------------------------------------------

ni = 1

while (ni<22):
    fo_out.write("*Node Print, Nset=R1-%d, Summary=No,
    freq=1 \n" % (ni))
    fo_out.write("U \n")
    fo_out.write("*Node Print, Nset=P1-%d, Summary=No,
    freq=1 \n" % (ni))
    fo_out.write("U \n")
    fo_out.write("*Node Print, Nset=R2-%d, Summary=No,
    freq=1 \n" % (ni))
    fo_out.write("U \n")
    fo_out.write("*Node Print, Nset=P2-%d, Summary=No,
    freq=1 \n" % (ni))
    fo_out.write("U \n")
    fo_out.write("*Node Print, Nset=Q1-%d, Summary=No,
    freq=1 \n" % (ni))
    fo_out.write("U \n")
    fo_out.write("*Node Print, Nset=S1-%d, Summary=No,
    freq=1 \n" % (ni))
    fo_out.write("U \n")
    fo_out.write("*Node Print, Nset=Q2-%d, Summary=No,
    freq=1 \n" % (ni))
    fo_out.write("U \n")
    fo_out.write("*Node Print, Nset=S2-%d, Summary=No,
    freq=1 \n" % (ni))
    fo_out.write("U \n")
    ni += 1

fo_out.close()
```

Appendix B

Abaqus Input Files

B.1 Mode 1 - Traction Coefficient Extraction Model

```
**----------------------------------------------------------------
** MATERIAL PROPERTY DEFINITION\\
**----------------------------------------------------------------
*Material, name=Material-1
*Damage Initiation, criterion=MAXPS
 65.5,
*Damage Evolution, type=DISPLACEMENT
 0.01,
*Elastic
3390., 0.41
*Initial Conditions, type=ENRICHMENT
specimen-1.15050, 1,Crack-1, -0.00999999, -0.00999999
specimen-1.15050, 2,Crack-1, 1e-06, -0.00999999
specimen-1.15050, 3,Crack-1, 1e-06, -0.00999999
specimen-1.15050, 4,Crack-1, -0.00999999, -0.00999999
specimen-1.15050, 5,Crack-1, -0.00999999, 0.
specimen-1.15050, 6,Crack-1, 1e-06, 0.
....... .......
specimen-1.19950, 3,Crack-1, 1e-06
specimen-1.19950, 4,Crack-1, -0.00999999
specimen-1.19950, 5,Crack-1, -0.00999999
specimen-1.19950, 6,Crack-1, 1e-06
specimen-1.19950, 7,Crack-1, 1e-06
specimen-1.19950, 8,Crack-1, -0.00999999
```

```
**----------------------------------------------------------------
** STEP: Step-1
**----------------------------------------------------------------
*Step, name=Step-1, nlgeom=NO
*Static
0.01, 1., 1e-35, 0.01
**----------------------------------------------------------------
** LOADS
**----------------------------------------------------------------
** Name: Load-1    Type: Pressure
*Dsload
Surf-1, P, -100.
** Name: Load-2    Type: Pressure
*Dsload
Surf-2, P, -100.
**----------------------------------------------------------------
** INTERACTIONS
**----------------------------------------------------------------
** Interaction: Int-1
*Enrichment Activation, name=Crack-1, activate=ON
**----------------------------------------------------------------
** CONTROLS
**----------------------------------------------------------------
*Controls, reset
*Controls, parameters=time incrementation
, , , , , , , , 20, , ,
**----------------------------------------------------------------
** OUTPUT REQUESTS
**----------------------------------------------------------------
*Restart, write, frequency=0
**----------------------------------------------------------------
** FIELD OUTPUT: F-Output-1
**----------------------------------------------------------------
*Output, field
*Node Output
CF, PHILSM, PSILSM, RF, U
```

```
*Element Output, directions=YES
LE, PE, PEEQ, PEMAG, S, STATUS, STATUSXFEM
*Contact Output
CDISP, CSTRESS
**--------------------------------------------------------------
** HISTORY OUTPUT: H-Output-1
**--------------------------------------------------------------
*Output, history, variable=PRESELECT
*End Step
```

B.2 RUC simulation model

```
**--------------------------------------------------------------
** MATERIALS
**--------------------------------------------------------------
*Material, name=MAT0
*Damping, alpha=3.75e+06
*Density
 1.37e-09,
*Depvar
      5,
*Elastic
 3.39e+09, 0.41
*Material, name=MAT1
*Damping, alpha=3.75e+06
*Density
 1.37e-09,
*Depvar
      5,
*Elastic, type=ENGINEERING CONSTANTS
159520.,11660.,11660., 0.267, 0.267, 0.472, 3813., 3813.
 3961.,
**--------------------------------------------------------------
** INTERACTION PROPERTIES
**--------------------------------------------------------------
*Surface Interaction, name=YARN
1.,
```

```
*Friction, slip tolerance=0.005
 0.6,
*Cohesive Behavior, eligibility=SPECIFIED CONTACTS
 253722, 90561, 90561
*Damage Initiation, criterion=MAXS
 65.5, 65.5, 65.5
**
*Surface, type=ELEMENT, name=yarn_7_bottom
_yarn_7_bottom_S3, S3
** Constraint: Q1-2_S1-2_RXy
*Equation
3
Q1-2, 4, 1.
S1-2, 4, -1.
Node_X1-2, 4, 2.658
** Constraint: Q1-2_S1-2_RYy
*Equation
3
Q1-2, 5, 1.
S1-2, 5, -1.
Node_X1-2, 5, -2.658
....... .......
** Constraint: R2-20_P2-20_Vx
*Equation
3
R2-20, 2, 1.
P2-20, 2, -1.
Node_Y2-20, 2, -2.658
** Constraint: R2-20_P2-20_Zx
*Equation
3
R2-20, 3, 1.
P2-20, 3, -1.
Node_Y2-20, 3, 6.304117
*End Assembly
```

```
**----------------------------------------------------------------
** INTERACTIONS
**----------------------------------------------------------------
** Interaction: yarn 0,2 -1
*Contact Pair, interaction=YARN, small sliding,
type=SURFACE TO SURFACE
s_Surf-17, m_Surf-17
*Initial Conditions, type=CONTACT
s_Surf-17, m_Surf-17,
** Interaction: yarn 0,3 - 2
....... .......
*Contact Pair, interaction=YARN, small sliding,
type=SURFACE TO SURFACE
yarn_5_bottom, yarn_6_top
*Initial Conditions, type=CONTACT
yarn_5_bottom, yarn_6_top,
** Interaction: yarn 7,0 - 9
*Contact Pair, interaction=YARN, small sliding,
type=SURFACE TO SURFACE
s_Surf-33, yarn_0_top
*Initial Conditions, type=CONTACT
s_Surf-33, yarn_0_top,
**----------------------------------------------------------------
** STEP: Step-1
**----------------------------------------------------------------
*Step, name=Step-1, nlgeom=YES, inc=1000
*Static
0.1, 1., 1e-35, 0.1
**----------------------------------------------------------------
** BOUNDARY CONDITIONS
**----------------------------------------------------------------
** Name: Node X1-set Type: Displacement/Rotation
*Boundary
Set-392, 1, 1
Set-392, 2, 2
Set-392, 3, 3
```

```
Set-392, 4, 4
Set-392, 5, 5
Set-392, 6, 6
....... .......
** Name: Node Y2-set Type: Displacement/Rotation
*Boundary
Set-395, 1, 1, 0.001
Set-395, 2, 2
Set-395, 3, 3
Set-395, 4, 4
Set-395, 5, 5
Set-395, 6, 6
**------------------------------------------------------------
** OUTPUT REQUESTS
**------------------------------------------------------------
*Restart, write, frequency=0
**------------------------------------------------------------
** FIELD OUTPUT: F-Output-1
**------------------------------------------------------------
*Output, field, variable=PRESELECT
**------------------------------------------------------------
** HISTORY OUTPUT: H-Output-1
**------------------------------------------------------------
*Output, history, variable=PRESELECT
*Node Print, Nset=Node_Y1-2, Summary=No, freq=1
RF
*Node Print, Nset=Node_Y2-2, Summary=No, freq=1
RF
*Node Print, Nset=Node_X1-2, Summary=No, freq=1
RF
*Node Print, Nset=Node_X2-2, Summary=No, freq=1
RF
....... .......
*Node Print, Nset=R1-20, Summary=No, freq=1
U
*Node Print, Nset=P1-20, Summary=No, freq=1
```

```
U
*Node Print, Nset=R2-20, Summary=No, freq=1
U
*Node Print, Nset=P2-20, Summary=No, freq=1
U
*Node Print, Nset=Q1-20, Summary=No, freq=1
U
*Node Print, Nset=S1-20, Summary=No, freq=1
U
*Node Print, Nset=Q2-20, Summary=No, freq=1
U
*Node Print, Nset=S2-20, Summary=No, freq=1
U
*End Step
```

Appendix C

MATLAB Script for Post-Processing

```
vf=[]; %virtual force matrix
vd=[]; %virtual displacement matrix

conv_R=[1 0 0 0 0 0;0 1 0 0 0 0;0 0 -1 0 0 0;0 0 0 -1 0 0;
        0 0 0 0 1 0;0 0 0 0 0 1];
conv_P=[-1 0 0 0 0 0;0 -1 0 0 0 0;0 0 -1 0 0 0;0 0 0 -1 0 0;
         0 0 0 0 -1 0;0 0 0 0 0 -1];

eq_S1Q1 = [0.702959 0.817226 0.931953 1.046861 1.161876
           1.276922 1.391987 1.507083 1.622188 1.737301
           1.852413 1.967521 2.082615 2.197682 2.312728
           2.427743 2.542648 2.657378 2.771645];
eq_S2Q2 = [4.235438 4.349708 4.464435 4.579341 4.694352
           4.809391 4.924482 5.039573 5.154665 5.269783
           5.384901 5.499992 5.615083 5.730175 5.845213
           5.960225 6.07513  6.189849 6.304117];
eq_P1R1 = [0.702956 0.817223 0.931953 1.046859 1.161873
           1.276919 1.391987 1.507081 1.622188 1.737301
           1.852413 1.967518 2.082615 2.19768 2.312726
           2.42774  2.542648 2.657375 2.771643];
eq_P2R2 = [4.235438 4.349705 4.464435 4.579341 4.694352
           4.809391 4.924482 5.039573 5.154665 5.269783
           5.384901 5.499992 5.615083 5.730175 5.845213
           5.960225 6.07513  6.189849 6.304117];
```

```
for file=1:6

    filenumber=int2str(file);
    filename=['Test_',filenumber,'.txt'];

    %read outputs from the text files
    [a1,b1,c1,d1,e1,f1,g1,h1,i1,j1,k1,l1]=
    textread(filename,'%s %s %s %s %s %s %s %s %s %s
    %s %s',912);
    data=[b1 c1 d1 e1 f1 g1];
    impo=data;
    R1=[];
    P1=[];
    bb=[]; % Keeping 48 reaction forces (column matrix)
    X1=[];
    i=1;
    p=4;
    g=1;

    while p<306

        i = ceil(p/16);

        t1=[1/2.658 0 0 0 0 0;0 0.5/1.329 0 0 0 0;
        0 0 1/eq_P1R1(1,i) 0 0 0;0 0 0 0.5/1.329 0 0;
        0 0 0 0 1/2.658 0;0 0 0 0 0 1];
        t2=[1/2.658 0 0 0 0 0;0 0.5/1.329 0 0 0 0;
        0 0 1/eq_P2R2(1,i) 0 0 0;0 0 0 0.5/1.329 0 0;
        0 0 0 0 1/2.658 0;0 0 0 0 0 1];
        t3=[0.5/1.329 0 0 0 0 0;0 1/2.658 0 0 0 0;
        0 0 1/eq_S1Q1(1,i) 0 0 0;0 0 0 1/2.658 0 0;
        0 0 0 0 0.5/1.329 0;0 0 0 0 0 1];
        t4=[0.5/1.329 0 0 0 0 0;0 1/2.658 0 0 0 0;
        0 0 1/eq_S2Q2(1,i) 0 0 0;0 0 0 1/2.658 0 0;
        0 0 0 0 0.5/1.329 0;0 0 0 0 0 1];
```

```
        R1(:,1)=str2double(data(p,:));
        R1=conv_R*R1;
        if rem(g,4)==1
            X1=t1*R1;
        elseif rem(g,4)==2
            X1=t2*R1;
        elseif rem(g,4)==3
            X1=t3*R1;
        elseif rem(g,4)==0
            X1=t4*R1;
        end

        bb=[bb;X1];

        P1=conv_P*R1;
          if rem(g,4)==1
            P1=t1*P1;
        elseif rem(g,4)==2
            P1=t2*P1;
        elseif rem(g,4)==3
            P1=t3*P1;
        elseif rem(g,4)==0
            P1=t4*P1;
        end
        bb=[bb;P1];

        p=p+4;
        g=g+1;
        i=i+1;

    end

    vf=[vf bb]; %Virtual Force Matrix

    UR=[]; %Virtual Displacemnts U1,U2,U3,UR1,UR2,UR3
    cc=[]; %Keeping 48 Displacemet values
```

```
    t=308;
    while t<913
        UR(:,1)=str2double(data(t,:));
        cc=[cc;UR];

        t=t+4;
    end
    vd=[vd cc];

    D=1/7.064964;

    Matrix=transpose(vd)*vf;
    ABD_Matrixi=D*Matrix;

end

 ABD_Matrixi
    A = ABD_Matrixi(1:3,1:3);
    a = inv(A);
    A11 = 1/a(1,1)
    A22 = 1/a(2,2)
    A12 = 1/a(1,2)
```